

# Fracture of Pipelines and Cylinders Containing a Circumferential Crack

by F. Erdogan and H. Ezzat

## CONTENTS

Abstract .....	1
1. Introduction .....	1
1.1 Fracture Mechanics Approach .....	1
1.2 Brief Survey of the Field .....	2
1.3 Circumferential Flaws .....	3
2. Stress Intensity Factors .....	3
2.1 Results for a Surface Crack .....	3
2.2 Stress Intensity Factors for a Through Crack .....	6
3. Crack Opening Displacement .....	9
4. The Pipe Experiments .....	10
4.1 Stresses in a Pipe under "Four Point" Bending .....	11
4.2 Mechanical Properties of the Material ..	12
4.3 The Fatigue Experiments .....	13
4.4 Fracture Tests .....	14
4.5 Examination of Fracture Surfaces .....	18
5. Conclusions .....	19
6. References .....	23
7. Acknowledgments .....	23

## Abstract

This study is concerned with the problem of a pipe containing a part-through or a through circumferential crack. First, the stress intensity factors for an internal or an external circumferential surface crack in a pipe are obtained. The main objective here is to give the necessary theoretical information for the treatment of subcritical crack growth process. Next the problem of a through crack in the presence of large scale plastic deformations is considered. The crack opening displacement (COD) is used as the main parameter to analyze the fracture instability problem and to correlate the experimental results. In the analytical part of the study Reissner's shell theory and an elastic or elastic-plastic line spring model are used to formulate the problem. The experiments were performed on 20-inch diameter X60 line pipes. A 0.025-inch wide starter notch was introduced to the pipes which were then subjected to cyclic loading under four point bending. The limited data obtained from the fatigue tests give the expected result, namely that the crack propagation rate in pipes may be predicted from the baseline data obtained from simple specimens provided the stress intensity factors for pipes are calculated with sufficient accuracy. The ductile fracture re-

F. Erdogan is Professor of Mechanics, Lehigh University, Bethlehem, Pa., H. Ezzat is Assistant Professor of Mechanical Engineering, University of Pittsburgh, Pa.

The research reported in this paper was supported by the U.S. Department of Transportation, Office of University Research.

Publication of this report was sponsored by the Weldability Committee of the Welding Research Committee.

sults show that the technique based on the asymptotic behavior of COD may be quite useful in determining a conservative estimate of the fracture instability load.

## 1. Introduction

This report presents the theoretical and the experimental results of a four year study on the fracture of circumferentially cracked pipelines and relatively thin-walled cylindrical containers. The research was sponsored by the U.S. Department of Transportation, Research and Special Programs Administration, Office of University Research. It was part of a coordinated DOT program in which the National Bureau of Standards and Johns Hopkins University were the other participants.

The primary objective of the research program was (a) to identify the possible modes of fracture failure in pipelines and in relatively thin-walled cylindrical containers containing various types of initial circumferential flaws, (b) to review and develop appropriate fracture criteria and to carry out the necessary analytical investigations which may be applied to various phases of fracture failure in circumferentially cracked pipes and containers, and (c) to design and perform an experimental research program in order to test the validity of the related analytical models.

### 1.1 Fracture Mechanics Approach

Depending on the thermo-mechanical behavior of the material and the nature of applied loads and environmental conditions, in the design of pipelines, tank cars, and a variety of other pressurized containers, it is often necessary to consider fatigue or corrosion crack propagation and fracture among the possible modes of failure. This requires, in addition to the application of standard failure theories specified by the existing design codes, the treatment of the problem of acceptance and safety from the viewpoint of fracture mechanics. In using this approach the flaws or certain types of imperfections which may initially exist in the material are treated as "cracks." These initial flaws which may have the potential of growing into a macroscopic fatigue or corrosion fatigue crack are generally weld defects (such as slag inclusions, excessive or inadequate weld penetration, incomplete fusion, gas pockets, arc burns, etc.), notches caused by possible initial misalignment during

welding, accidental dents, scratches, or gouges put on the pipe or the cylinder during manufacturing and transportation, and accidental damages which occur during the period of operation. Thus, in designing pipelines and pressurized containers used for transporting goods a safe design philosophy requires that the existence of such defects be taken into consideration.

Fracture mechanics approach has been highly successful in dealing with this so-called fracture control problem which involves subcritical propagation of fatigue and stress corrosion cracks, brittle or quasi-brittle fracture, and ductile fracture. In a broad sense the objective of the pipeline and container fracture analysis is the determination of the maximum allowable initial flaw size (of certain specified shape, location and orientation) which would not grow into a crack going through the entire thickness of the cylinder wall under a specified load history and environmental conditions. The general procedure for the fracture analysis may be outlined as follows:

- (a) The strength characterization of the material with regard to fatigue and corrosion fatigue crack propagation, stress corrosion cracking, brittle or quasi-brittle fracture, and ductile or post-yield fracture.
- (b) Determination of the time profile of all significant external loads and operating temperature and a complete stress analysis (including the residual stresses) of the structure by ignoring the existence of any flaws.
- (c) Obtaining the map of significant existing flaws by means of appropriate nondestructive flaw detection techniques, or making a realistic (and conservative) assumption regarding the location, size, and orientation of dominant flaws.
- (d) Performing the fracture analysis to estimate the life of the structure. Generally, this step requires the calculation of the relevant stress intensity factor and the use of a proper subcritical crack growth model to estimate the propagation rate of the part-through crack in the initial elastic range, the application of a modified crack growth model to estimate the crack propagation rate in the elastic-plastic range, and the use of an appropriate post-yield fracture criterion to estimate the critical net ligament thickness capable of sustaining the specified peak load.

## 1.2 Brief Survey of the Field

For the purpose of a brief review one may consider the research efforts regarding pipeline fracture analysis in the following categories: (i) theoretical work aimed at the calculation of quantities such as stress intensity factor, crack opening displacement, or  $J$ -integral which may be used in an appropriate fracture or fatigue theory as the representative of the external loads and flaw geometry, (ii) the theoretical and experimental work aimed at the development of proper "models," "criteria," or "theories" for fatigue crack propagation, corrosion fatigue, stress corrosion cracking, and fracture

in pipeline materials, (iii) experimental work aimed at the verification or demonstration of the related theories in pipes, including crack morphology studies, (iv) dynamics of crack propagation in pipelines. The technical literature in the field is quite extensive (see, for example, Ref. 1 for an extensive list of references and a critical review). Most of the theoretical work in category (i) which is relevant to pipeline studies has been on the elastic solutions for part-through cracks in plates and for through cracks in shells. Some of the significant solutions and results regarding the part-through cracks in plates may be found in Ref. 2. A review of the more recent studies and rather accurate finite element results may be found in Ref. 3. The problem of a through crack in cylindrical and spherical shells has been discussed in a review article, Ref. 4, where, in addition to a nearly complete list of references, a summary of the existing results has been included. The plasticity effects in cylindrical shells with an axial crack have been considered in Ref. 5. Reference 6 summarizes some of the recent approximate and finite element results on the thick-walled cylinders with a part-through crack.

The processes of brittle and quasi-brittle fracture, and the subcritical crack propagation due to fatigue, corrosion fatigue, and stress corrosion cracking appear to be, at least from an empirical viewpoint, well-understood and the models dealing with such phenomena have been adequately standardized (see, for example, Ref. 7). The stress intensity factor is almost universally accepted and used as the primary correlation parameter in all these models. However, in the presence of relatively large scale plastic deformations the effects of specimen and crack geometry, elastic-plastic stress-strain behavior of the material, and the nature of the external loads on the fracture initiation and propagation is much too great to permit the treatment of the phenomenon by means of a single parameter (such as  $K_{IC}$ ,  $G_{IC}$ , or  $J_{IC}$ ). Thus, the relatively successful ductile fracture models contain generally more than one material constant. For example, the crack extension resistance curve ( $R$  of  $K_R$  - curve)<sup>8</sup> is a continuously distributed parameter model and Newman's criterion<sup>9</sup> is a two-parameter model. A discussion of these and other ductile fracture models and related references may be found in the review article.<sup>10</sup> A good deal of work on pipeline fracture has been done at Battelle-Columbus Laboratories. A partial summary of the results and the techniques used in these studies may be found in Ref. 11 and an extensive review of fracture mechanics approaches dealing with girth weld discontinuities is given in Refs. 12 and 13.

The importance of dynamic problems lies in the fact that in natural gas pipelines once the axial through crack appears in the pipe wall it rapidly grows and reaches a velocity which is generally greater than the decompression wave velocity of the gas in the pipe. Hence, the crack is subjected to a constant driving force and, unless it is arrested by some obstacle or is diverted in the hoop direction, it may run rather long distances causing considerable damage to the surroundings. The

papers in Reference 14 provide a good sampling of the work in this area (see also Ref. 15 for more recent work and references, and Ref. 16 for work in finite volume containers).

### 1.3 Circumferential Flaws

In pressure vessels and piping generally the primary load component is the internal pressure. Consequently, in the past considerable emphasis has been placed on the studies of fracture problems arising from axial flaws in the cylinder (see, for example, Refs. 11 and 14 for typical fracture studies and Refs. 17–21 for the elastic solutions of through and part-through axial crack problems in cylinders). On the other hand, particularly in piping, the secondary loads are mostly axial and generally time-dependent. Relatively high frequency and low amplitude flow-induced vibrations in heat exchanger tubing and in line pipes near the pumping stations may be cited as some examples. Severe bending in pipes due to fit-up or that in offshore piping while laying off the barge, and variety of constraint stresses caused by thermal fluctuations, ground settlements, and earthquakes may be mentioned as examples of axial loading with very low frequency and relatively high amplitude (see, for example, Refs. 12, 13, 21, 22, and 23 for sample studies).

From the viewpoint of analytical modeling the fatigue crack propagation and fracture problems in pressure vessels and piping may be considered in three loose groupings. The first is the problem of fatigue crack propagation and fracture in pipes or cylinders having a dominant part-through or through crack in which the plastic deformations are confined to a small region along the crack front [Fig. 1(a) and (b)]. In such problems the stress intensity factor appears to be highly satisfactory as the correlation parameter and hence an elastic solution of the related crack problem is sufficient for the fracture or fatigue analysis. The second group relates to the "ductile fracture" problems which involve extensive plastic deformations around the crack front through the net ligament [Fig. 1(c)]. In this case a variety of parameters or criteria (such as COD, CTOD,  $J$  integral  $J_R$ -curve, net ligament plastic strain instability, and plastic collapse load) are used to analyze the fracture initiation, stable crack growth, and unstable fracture. However, particularly in piping and other relatively thin-walled components this ductile fracture process seems to be very highly dependent on the gross mechanics of the structure. Therefore, no single parameter criterion ignoring the relevant aspects of the overall mechanics problem would be adequate to model the process. The third group is concerned with the dynamic fracture propagation in pipelines which may follow the instability of an axial crack.

In this paper, after a brief outline of the technique used to analyze the problem, first some calculated stress intensity factors for a circumferential part-through crack in cylinders are presented. With a proper subcritical crack growth model and appropriate baseline data, these results may be used to estimate fatigue or

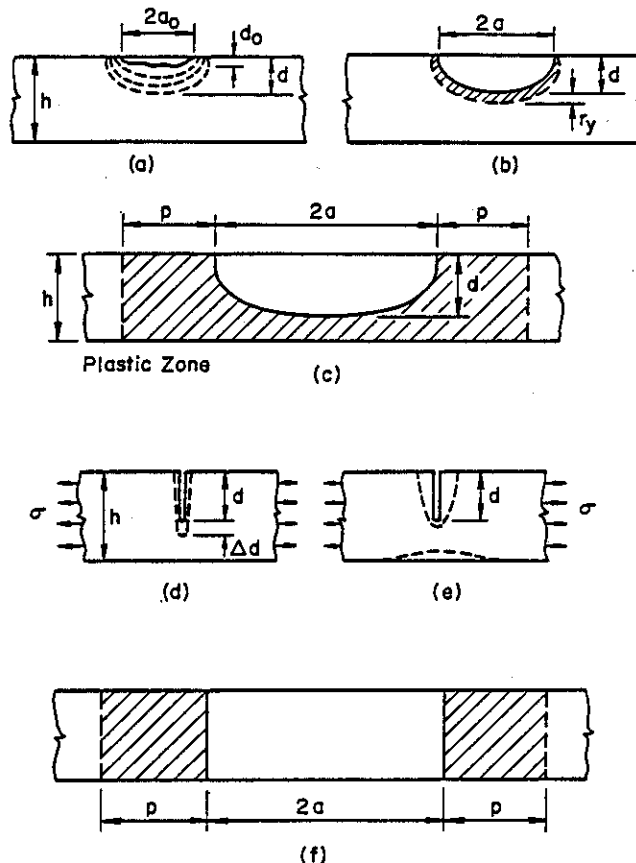


Fig. 1—Evolution of a through crack. (a) initial flaw and subcritical crack propagation, (b) part-through crack with confined plastic zone and largely elastic net ligament, (c) part-through crack with fully yielded net ligament, (d) progressive growth of part-through crack, (e) plastic necking of the net ligament, (f) through crack with relatively large plastic zones

corrosion fatigue crack propagation rate in the cylinder. Next, some sample results obtained from the elastic-plastic solution of pipes having a relatively large crack with a fully yielded net ligament are given and their possible use in estimating the fracture initiation and instability loads is discussed. Finally, the experimental results on the fatigue crack propagation and fracture of a 20-inch diameter line pipe tested under four point bending are presented and discussed.

## 2. Stress Intensity Factors

### 2.1 Results for a Surface Crack

The general formulation of the cylindrical shell containing an axial or a circumferential through crack was given in Ref. 22. In this study Reissner's transverse shear theory was used to formulate the problem. The corresponding part-through crack problem was considered in Ref. 21. In this section additional axial and circumferential crack results for certain standard line pipes as well as some results for spirally oriented cracks are given.

The basic geometry of the shell with a circumferential crack is given in Fig. 2. In most cases the stress state in the neighborhood of the crack is approximately uniform. Thus, if the loading is symmetric with respect to the

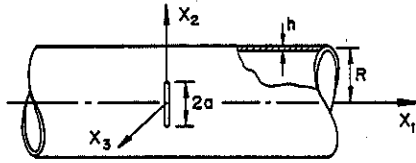


Fig. 2—The cylinder with a circumferential through crack

plane of the crack, the problem may be solved by assuming that

$$N_{11}(X_2) = N_{\infty} = \text{constant}, M_{11}(X_2) = 0, \text{ or } (1)$$

$$M_{11}(X_2) = M_{\infty} = \text{constant}, N_{11}(X_2) = 0, (2)$$

where  $N_{11}$  and  $M_{11}$  are respectively the membrane and bending resultants. Aside from the uniform loading given by Eqs. 1 and 2, in pipes the loading which is of considerable practical interest is the gross bending with bending moment  $M_0$  at the cracked section  $X_1 = 0$  (Fig. 2). In this case in the absence of crack the stress in the cylinder may be expressed as

$$\sigma_{11} = \frac{M_0 z_0}{I} = \frac{M_0 R}{I} \left(1 - \frac{X_2^2}{2R^2}\right) + \frac{M_0 X_3}{I} \left(1 - \frac{X_2^2}{2R^2}\right), I = Rh(4R^2 + h^2) (3)$$

where  $z_0$  is the distance from the neutral plane. Thus, by observing that local membrane and bending stresses are related to the stress and moment resultants by

$$\sigma_{11}^m = N_{11}/h, \sigma_{11}^b = 12 M_{11} X_3 / h^3, (4)$$

and by letting  $\sigma_{11} = \sigma_{11}^m + \sigma_{11}^b$ , from Eqs. 3 and 4 we obtain the resultants which are to be used as external loads in the crack problem as follows:

$$N_{11}(X_2) = \frac{M_0 R h}{I} \left(1 - \frac{X_2^2}{2R^2}\right) = N_{\infty} \left(1 - \frac{X_2^2}{2R^2}\right), (5)$$

$$M_{11}(X_2) = \frac{M_0 h^3}{12I} \left(1 - \frac{X_2^2}{2R^2}\right) = M_{\infty} \left(1 - \frac{X_2^2}{2R^2}\right). (6)$$

Sample results giving the stress intensity factor at the maximum penetration point  $L = L_0$  of a semielliptic inner or outer circumferential crack in standard line pipes are given in Tables 1–8 (see the insert in Fig. 21). Similar results for the semi-elliptic axial inner or outer surface crack may be found in Ref. 24. Additional general results for surface cracks in cylindrical shells in terms of the dimensionless variables  $L_0/h$ ,  $a/h$  and  $\lambda = [12(1 - \nu^2)]^{1/4} a / \sqrt{Rh}$  are given in Ref. 21. Reference 21 also contains the stress intensity factors for a surface crack in the cylinder subjected to local bending of the shell wall. The analysis used for the calculation of stress intensity factors is based on the Reissner's shell theory and the elastic line spring model and is described in Refs. 21, 22 and 24 in detail. Reference 21 gives a spot comparison of the analytical results obtained from the

Table 1.  $K/K_0$  in a line pipe with OD = 48 in.,  $h = 0.625$  in.

$L_0/h$	0.1	0.2	0.3	0.4	0.5	0.6	0.7	0.8	0.9
Outer circumferential crack, $N_{\infty} \neq 0, M_{\infty} = 0$									
1.0	0.945	0.817	0.664	0.508	0.366	0.247	0.147	0.074	0.033
2.0	0.967	0.882	0.766	0.628	0.481	0.340	0.209	0.106	0.048
3.0	0.976	0.911	0.817	0.695	0.554	0.405	0.257	0.132	0.060
4.0	0.980	0.928	0.848	0.739	0.605	0.455	0.296	0.155	0.070
5.0	0.983	0.939	0.868	0.770	0.643	0.494	0.329	0.175	0.079
6.0	0.985	0.946	0.882	0.792	0.672	0.525	0.357	0.193	0.088
7.0	0.987	0.951	0.893	0.809	0.694	0.551	0.381	0.209	0.096
8.0	0.988	0.954	0.900	0.821	0.712	0.572	0.401	0.223	0.104
Outer circumferential crack, $N_{\infty} = 0, M_{\infty} \neq 0$									
1.0	0.944	0.805	0.627	0.443	0.273	0.133	0.040	-0.011	-0.034
2.0	0.966	0.874	0.741	0.581	0.407	0.242	0.109	0.020	-0.028
3.0	0.975	0.906	0.798	0.658	0.492	0.318	0.163	0.047	-0.021
4.0	0.980	0.923	0.832	0.708	0.551	0.377	0.209	0.072	-0.017
5.0	0.983	0.934	0.855	0.742	0.595	0.422	0.246	0.094	-0.004
6.0	0.985	0.942	0.870	0.767	0.628	0.485	0.278	0.114	0.004
7.0	0.986	0.947	0.882	0.785	0.653	0.488	0.304	0.131	0.012
8.0	0.987	0.951	0.890	0.800	0.673	0.511	0.327	0.147	0.020
Inner circumferential crack, $N_{\infty} \neq 0, M_{\infty} = 0$									
1.0	0.944	0.814	0.660	0.503	0.361	0.243	0.145	0.073	0.033
2.0	0.965	0.877	0.757	0.616	0.468	0.328	0.202	0.102	0.048
3.0	0.974	0.905	0.804	0.677	0.532	0.384	0.242	0.124	0.058
4.0	0.978	0.920	0.832	0.716	0.575	0.425	0.273	0.142	0.066
5.0	0.981	0.930	0.850	0.742	0.607	0.456	0.297	0.156	0.073
6.0	0.983	0.937	0.864	0.762	0.631	0.480	0.318	0.169	0.080
7.0	0.984	0.941	0.873	0.776	0.650	0.500	0.335	0.180	0.086
8.0	0.985	0.945	0.880	0.787	0.664	0.517	0.350	0.190	0.091
Inner circumferential crack, $N_{\infty} = 0, M_{\infty} \neq 0$									
1.0	0.943	0.801	0.621	0.436	0.267	0.129	0.037	-0.012	-0.034
2.0	0.964	0.869	0.730	0.566	0.391	0.227	0.099	0.015	-0.030
3.0	0.973	0.898	0.783	0.635	0.465	0.292	0.144	0.037	-0.024
4.0	0.978	0.915	0.814	0.679	0.516	0.339	0.179	0.056	-0.018
5.0	0.981	0.925	0.835	0.709	0.552	0.375	0.207	0.071	-0.013
6.0	0.982	0.932	0.849	0.731	0.579	0.403	0.230	0.085	-0.007
7.0	0.984	0.937	0.859	0.747	0.600	0.426	0.249	0.096	-0.002
8.0	0.985	0.941	0.867	0.759	0.616	0.444	0.265	0.107	0.003

Table 2.  $K/K_0$  in a line pipe with OD = 48 in.,  $h = 0.75$  in.

$L_0/h$	0.1	0.2	0.3	0.4	0.5	0.6	0.7	0.8	0.9
Outer circumferential crack, $N_{\infty} \neq 0, M_{\infty} = 0$									
1.0	0.945	0.817	0.664	0.508	0.366	0.247	0.147	0.074	0.033
2.0	0.967	0.882	0.766	0.628	0.481	0.340	0.210	0.106	0.048
3.0	0.976	0.911	0.816	0.695	0.553	0.405	0.258	0.133	0.060
4.0	0.980	0.927	0.847	0.738	0.604	0.454	0.297	0.156	0.070
5.0	0.983	0.938	0.867	0.768	0.641	0.493	0.329	0.176	0.080
6.0	0.985	0.944	0.881	0.790	0.669	0.523	0.356	0.193	0.089
7.0	0.986	0.949	0.890	0.805	0.690	0.548	0.379	0.209	0.097
8.0	0.987	0.952	0.897	0.817	0.707	0.567	0.398	0.222	0.105
Outer circumferential crack, $N_{\infty} = 0, M_{\infty} \neq 0$									
1.0	0.944	0.805	0.627	0.443	0.273	0.133	0.040	-0.011	-0.034
2.0	0.966	0.874	0.741	0.580	0.407	0.242	0.110	0.020	-0.028
3.0	0.975	0.905	0.797	0.657	0.492	0.318	0.164	0.048	-0.020
4.0	0.980	0.922	0.831	0.706	0.550	0.376	0.209	0.073	-0.012
5.0	0.983	0.933	0.853	0.740	0.593	0.421	0.246	0.095	-0.003
6.0	0.985	0.941	0.868	0.764	0.624	0.456	0.276	0.114	0.006
7.0	0.986	0.946	0.879	0.781	0.648	0.483	0.302	0.131	0.014
8.0	0.987	0.949	0.886	0.794	0.666	0.505	0.323	0.146	0.021
Inner circumferential crack, $N_{\infty} \neq 0, M_{\infty} = 0$									
1.0	0.944	0.814	0.659	0.502	0.361	0.243	0.145	0.073	0.033
2.0	0.965	0.876	0.755	0.614	0.466	0.327	0.201	0.102	0.048
3.0	0.973	0.903	0.802	0.674	0.529	0.382	0.240	0.124	0.058
4.0	0.978	0.919	0.829	0.712	0.571	0.421	0.270	0.141	0.066
5.0	0.981	0.928	0.847	0.737	0.602	0.451	0.294	0.155	0.074
6.0	0.982	0.934	0.860	0.756	0.625	0.475	0.314	0.168	0.080
7.0	0.984	0.939	0.869	0.770	0.642	0.493	0.330	0.178	0.086
8.0	0.985	0.942	0.875	0.781	0.656	0.509	0.344	0.187	0.091
Inner circumferential crack, $N_{\infty} = 0, M_{\infty} \neq 0$									
1.0	0.943	0.801	0.621	0.436	0.266	0.128	0.037	-0.013	-0.034
2.0	0.964	0.868	0.729	0.563	0.389	0.225	0.098	0.015	-0.030
3.0	0.973	0.897	0.780	0.632	0.461	0.289	0.142	0.036	-0.024
4.0	0.977	0.913	0.811	0.675	0.510	0.335	0.176	0.054	-0.018
5.0	0.980	0.923	0.831	0.704	0.545	0.369	0.203	0.070	-0.012
6.0	0.982	0.930	0.844	0.724	0.571	0.396	0.224	0.082	-0.007
7.0	0.983	0.934	0.854	0.740	0.591	0.417	0.243	0.094	-0.002
8.0	0.984	0.938	0.861	0.751	0.606	0.434	0.258	0.104	0.003

Table 3.  $K/K_0$  in a line pipe with OD = 36 in.,  $h = 0.5$  in.

$L_0/h$	0.1	0.2	0.3	0.4	0.5	0.6	0.7	0.8	0.9
Outer circumferential crack, $N_{\theta} \neq 0, M_{\theta} = 0$									
1.0	0.945	0.817	0.664	0.508	0.366	0.247	0.147	0.073	0.033
2.0	0.967	0.882	0.766	0.628	0.481	0.340	0.210	0.106	0.048
3.0	0.976	0.911	0.817	0.695	0.554	0.405	0.257	0.132	0.060
4.0	0.980	0.928	0.848	0.739	0.605	0.455	0.297	0.155	0.070
5.0	0.983	0.938	0.868	0.769	0.642	0.494	0.330	0.175	0.079
6.0	0.985	0.945	0.882	0.791	0.671	0.525	0.357	0.193	0.088
7.0	0.987	0.950	0.892	0.808	0.693	0.550	0.380	0.209	0.096
8.0	0.988	0.954	0.900	0.820	0.710	0.570	0.400	0.223	0.104
Outer circumferential crack, $N_{\theta} = 0, M_{\theta} \neq 0$									
1.0	0.944	0.805	0.627	0.443	0.273	0.133	0.040	-0.011	-0.034
2.0	0.966	0.874	0.741	0.581	0.407	0.242	0.109	0.020	-0.028
3.0	0.975	0.905	0.798	0.657	0.492	0.318	0.164	0.048	-0.021
4.0	0.980	0.923	0.832	0.707	0.551	0.376	0.209	0.072	-0.012
5.0	0.983	0.934	0.854	0.741	0.594	0.422	0.246	0.094	-0.004
6.0	0.985	0.941	0.870	0.766	0.627	0.458	0.277	0.114	0.005
7.0	0.986	0.947	0.881	0.784	0.652	0.486	0.304	0.131	0.013
8.0	0.987	0.950	0.889	0.798	0.671	0.509	0.326	0.146	0.020
Inner circumferential crack, $N_{\theta} \neq 0, M_{\theta} = 0$									
1.0	0.944	0.814	0.659	0.503	0.361	0.243	0.145	0.073	0.033
2.0	0.965	0.877	0.756	0.615	0.467	0.328	0.201	0.102	0.048
3.0	0.974	0.904	0.803	0.676	0.531	0.383	0.241	0.124	0.058
4.0	0.978	0.920	0.831	0.714	0.574	0.424	0.272	0.142	0.066
5.0	0.981	0.929	0.850	0.741	0.605	0.454	0.296	0.156	0.074
6.0	0.983	0.936	0.862	0.760	0.629	0.478	0.316	0.169	0.080
7.0	0.984	0.940	0.872	0.774	0.647	0.498	0.333	0.179	0.086
8.0	0.985	0.944	0.879	0.785	0.662	0.514	0.348	0.189	0.091
Inner circumferential crack, $N_{\theta} = 0, M_{\theta} \neq 0$									
1.0	0.943	0.801	0.621	0.436	0.267	0.129	0.037	-0.012	-0.034
2.0	0.964	0.868	0.730	0.565	0.390	0.226	0.099	0.015	-0.030
3.0	0.973	0.898	0.782	0.634	0.464	0.291	0.143	0.037	-0.024
4.0	0.978	0.914	0.813	0.678	0.514	0.338	0.178	0.055	-0.018
5.0	0.980	0.924	0.833	0.707	0.549	0.373	0.205	0.071	-0.013
6.0	0.982	0.931	0.847	0.729	0.576	0.401	0.228	0.084	-0.007
7.0	0.984	0.936	0.857	0.745	0.597	0.423	0.247	0.095	-0.002
8.0	0.985	0.940	0.865	0.757	0.613	0.441	0.262	0.106	0.003

Table 4.  $K/K_0$  in a line pipe with OD = 36 in.,  $h = 0.625$  in.

$L_0/h$	0.1	0.2	0.3	0.4	0.5	0.6	0.7	0.8	0.9
Outer circumferential crack, $N_{\theta} \neq 0, M_{\theta} = 0$									
1.0	0.945	0.817	0.664	0.508	0.366	0.247	0.147	0.074	0.033
2.0	0.967	0.882	0.766	0.628	0.481	0.340	0.210	0.107	0.049
3.0	0.975	0.911	0.816	0.695	0.553	0.405	0.258	0.133	0.060
4.0	0.980	0.927	0.846	0.737	0.603	0.454	0.297	0.156	0.071
5.0	0.983	0.937	0.866	0.767	0.640	0.492	0.329	0.176	0.081
6.0	0.985	0.944	0.879	0.788	0.667	0.522	0.356	0.193	0.090
7.0	0.986	0.948	0.889	0.803	0.688	0.545	0.378	0.209	0.098
8.0	0.987	0.951	0.895	0.814	0.704	0.564	0.396	0.222	0.105
Outer circumferential crack, $N_{\theta} = 0, M_{\theta} \neq 0$									
1.0	0.944	0.805	0.627	0.443	0.273	0.134	0.040	-0.011	-0.034
2.0	0.966	0.874	0.741	0.580	0.407	0.242	0.110	0.021	-0.028
3.0	0.975	0.905	0.797	0.656	0.491	0.318	0.164	0.048	-0.020
4.0	0.980	0.922	0.830	0.705	0.549	0.375	0.209	0.073	-0.011
5.0	0.982	0.933	0.852	0.738	0.591	0.419	0.245	0.095	-0.002
6.0	0.984	0.940	0.866	0.761	0.622	0.453	0.275	0.114	0.006
7.0	0.986	0.944	0.877	0.778	0.645	0.480	0.300	0.130	0.014
8.0	0.986	0.948	0.884	0.790	0.662	0.491	0.320	0.145	0.022
Inner circumferential crack, $N_{\theta} \neq 0, M_{\theta} = 0$									
1.0	0.944	0.814	0.658	0.502	0.360	0.243	0.145	0.073	0.033
2.0	0.965	0.876	0.754	0.613	0.465	0.326	0.200	0.102	0.048
3.0	0.973	0.903	0.800	0.672	0.527	0.380	0.239	0.123	0.058
4.0	0.978	0.918	0.827	0.709	0.568	0.419	0.269	0.140	0.067
5.0	0.980	0.927	0.845	0.734	0.598	0.448	0.292	0.155	0.074
6.0	0.982	0.933	0.857	0.752	0.620	0.471	0.311	0.167	0.081
7.0	0.983	0.937	0.866	0.766	0.638	0.489	0.327	0.177	0.086
8.0	0.984	0.941	0.872	0.760	0.651	0.504	0.341	0.186	0.092
Inner circumferential crack, $N_{\theta} = 0, M_{\theta} \neq 0$									
1.0	0.942	0.801	0.620	0.435	0.266	0.128	0.037	-0.013	-0.034
2.0	0.964	0.867	0.727	0.562	0.397	0.224	0.097	0.015	-0.030
3.0	0.972	0.896	0.777	0.629	0.459	0.287	0.141	0.036	-0.024
4.0	0.977	0.912	0.809	0.671	0.507	0.332	0.174	0.054	-0.018
5.0	0.980	0.922	0.828	0.700	0.547	0.365	0.200	0.069	-0.012
6.0	0.981	0.928	0.841	0.720	0.566	0.391	0.221	0.081	-0.007
7.0	0.983	0.933	0.851	0.735	0.585	0.412	0.239	0.092	-0.001
8.0	0.984	0.936	0.858	0.746	0.600	0.429	0.254	0.102	0.004

Table 5.  $K/K_0$  in a line pipe with OD = 30 in.,  $h = 0.375$  in.

$L_0/h$	0.1	0.2	0.3	0.4	0.5	0.6	0.7	0.8	0.9
Outer circumferential crack, $N_{\theta} \neq 0, M_{\theta} = 0$									
1.0	0.945	0.817	0.664	0.508	0.366	0.247	0.147	0.073	0.033
2.0	0.967	0.883	0.766	0.628	0.481	0.340	0.209	0.106	0.048
3.0	0.976	0.912	0.817	0.696	0.554	0.405	0.257	0.132	0.060
4.0	0.981	0.928	0.848	0.740	0.605	0.455	0.296	0.158	0.070
5.0	0.983	0.939	0.869	0.770	0.643	0.494	0.329	0.175	0.078
6.0	0.985	0.946	0.883	0.793	0.672	0.526	0.357	0.193	0.088
7.0	0.987	0.951	0.893	0.810	0.695	0.552	0.381	0.209	0.096
8.0	0.988	0.954	0.901	0.822	0.713	0.573	0.401	0.223	0.103
Outer circumferential crack, $N_{\theta} = 0, M_{\theta} \neq 0$									
1.0	0.944	0.805	0.627	0.447	0.273	0.133	0.040	-0.011	-0.034
2.0	0.966	0.874	0.741	0.581	0.407	0.242	0.109	0.020	-0.028
3.0	0.975	0.906	0.798	0.658	0.492	0.318	0.163	0.047	-0.021
4.0	0.980	0.923	0.833	0.708	0.552	0.377	0.209	0.072	-0.013
5.0	0.983	0.935	0.855	0.743	0.595	0.423	0.246	0.094	-0.004
6.0	0.985	0.942	0.871	0.768	0.629	0.459	0.278	0.114	0.004
7.0	0.986	0.947	0.882	0.786	0.654	0.488	0.305	0.132	0.012
8.0	0.987	0.951	0.891	0.800	0.674	0.512	0.328	0.147	0.019
Inner circumferential crack, $N_{\theta} \neq 0, M_{\theta} = 0$									
1.0	0.944	0.815	0.660	0.503	0.361	0.243	0.145	0.073	0.033
2.0	0.965	0.878	0.757	0.616	0.468	0.328	0.202	0.103	0.048
3.0	0.974	0.905	0.805	0.677	0.532	0.385	0.242	0.124	0.058
4.0	0.978	0.921	0.833	0.716	0.576	0.426	0.273	0.142	0.066
5.0	0.981	0.930	0.852	0.743	0.608	0.457	0.298	0.157	0.073
6.0	0.983	0.937	0.865	0.763	0.632	0.482	0.319	0.169	0.080
7.0	0.984	0.942	0.874	0.778	0.651	0.502	0.336	0.181	0.086
8.0	0.985	0.945	0.881	0.789	0.666	0.518	0.351	0.190	0.091
Inner circumferential crack, $N_{\theta} = 0, M_{\theta} \neq 0$									
1.0	0.943	0.802	0.622	0.437	0.267	0.129	0.037	-0.012	-0.034
2.0	0.964	0.869	0.731	0.566	0.391	0.227	0.099	0.015	-0.030
3.0	0.973	0.898	0.784	0.636	0.466	0.293	0.144	0.037	-0.024
4.0	0.978	0.921	0.833	0.716	0.576	0.340	0.180	0.056	-0.018
5.0	0.981	0.925	0.836	0.712	0.553	0.377	0.208	0.072	-0.013
6.0	0.983	0.933	0.850	0.733	0.581	0.405	0.231	0.085	-0.007
7.0	0.984	0.938	0.860	0.749	0.602	0.428	0.250	0.097	-0.002
8.0	0.985	0.941	0.868	0.761	0.618	0.446	0.266	0.107	0.003

Table 6.  $K/K_0$  in a line pipe with OD = 30 in.,  $h = 0.5$  in.

$L_0/h$	0.1	0.2	0.3	0.4	0.5	0.6	0.7	0.8	0.9
Outer circumferential crack, $N_{\theta} \neq 0, M_{\theta} = 0$									
1.0	0.945	0.817	0.664	0.508	0.366	0.247	0.147	0.074	0.033
2.0	0.967	0.882	0.766	0.628	0.481	0.340	0.210	0.107	0.049
3.0	0.975	0.911	0.816	0.695	0.553	0.405	0.258	0.133	0.060
4.0	0.980	0.927	0.847	0.738	0.604	0.454	0.297	0.156	0.071
5.0	0.983	0.937	0.866	0.767	0.640	0.492	0.329	0.176	0.081
6.0	0.985	0.944	0.880	0.788	0.668	0.522	0.356	0.193	0.089
7.0	0.986	0.949	0.890	0.804	0.689	0.546	0.378	0.209	0.098
8.0	0.987	0.952	0.896	0.815	0.705	0.565	0.397	0.222	0.105
Outer circumferential crack, $N_{\theta} = 0, M_{\theta} \neq 0$									
1.0	0.944	0.805	0.627	0.443	0.273	0.134	0.040	-0.011	-0.034
2.0	0.9								

Table 7.  $K/K_0$  in a line pipe with OD = 24 in.,  $h = 0.344$  in.

$L_0/h$	0.1	0.2	0.3	0.4	0.5	0.6	0.7	0.8	0.9
Outer circumferential crack, $N_\infty=0, M_o=0$									
1.0	0.945	0.817	0.664	0.508	0.366	0.247	0.147	0.073	0.033
2.0	0.967	0.882	0.766	0.628	0.481	0.340	0.210	0.106	0.048
3.0	0.976	0.911	0.817	0.695	0.553	0.405	0.257	0.132	0.060
4.0	0.980	0.928	0.847	0.739	0.604	0.455	0.297	0.155	0.070
5.0	0.983	0.938	0.868	0.769	0.642	0.493	0.329	0.175	0.080
6.0	0.985	0.945	0.882	0.791	0.670	0.524	0.357	0.193	0.088
7.0	0.987	0.950	0.892	0.807	0.692	0.549	0.380	0.209	0.097
8.0	0.987	0.953	0.899	0.819	0.709	0.570	0.400	0.223	0.104
Outer circumferential crack, $N_\infty=0, M_o \neq 0$									
1.0	0.944	0.805	0.627	0.443	0.273	0.133	0.040	-0.011	-0.034
2.0	0.966	0.874	0.741	0.581	0.407	0.242	0.109	0.020	-0.028
3.0	0.975	0.905	0.798	0.657	0.492	0.318	0.164	0.048	-0.021
4.0	0.980	0.923	0.832	0.707	0.551	0.376	0.209	0.072	-0.012
5.0	0.983	0.934	0.854	0.741	0.594	0.421	0.246	0.094	-0.004
6.0	0.985	0.941	0.869	0.765	0.626	0.457	0.277	0.114	0.005
7.0	0.986	0.946	0.880	0.783	0.651	0.485	0.303	0.131	0.013
8.0	0.987	0.950	0.888	0.797	0.670	0.508	0.325	0.146	0.020
Inner circumferential crack, $N_\infty=0, M_o=0$									
1.0	0.944	0.814	0.659	0.503	0.361	0.243	0.145	0.073	0.033
2.0	0.965	0.877	0.756	0.615	0.467	0.327	0.201	0.102	0.048
3.0	0.974	0.904	0.803	0.675	0.530	0.383	0.241	0.124	0.058
4.0	0.978	0.919	0.831	0.714	0.573	0.423	0.271	0.141	0.066
5.0	0.981	0.929	0.849	0.740	0.604	0.453	0.296	0.156	0.074
6.0	0.983	0.935	0.862	0.759	0.628	0.477	0.316	0.168	0.080
7.0	0.984	0.940	0.871	0.773	0.646	0.497	0.332	0.179	0.086
8.0	0.985	0.943	0.878	0.784	0.660	0.513	0.347	0.189	0.091
Inner circumferential crack, $N_\infty=0, M_o \neq 0$									
1.0	0.943	0.801	0.621	0.436	0.267	0.129	0.037	-0.012	-0.034
2.0	0.964	0.868	0.729	0.565	0.390	0.225	0.099	0.015	-0.030
3.0	0.973	0.897	0.782	0.634	0.463	0.291	0.143	0.037	-0.024
4.0	0.977	0.914	0.813	0.677	0.513	0.337	0.177	0.055	-0.018
5.0	0.980	0.924	0.833	0.706	0.548	0.372	0.204	0.070	-0.012
6.0	0.982	0.931	0.846	0.728	0.575	0.399	0.227	0.084	-0.007
7.0	0.983	0.936	0.856	0.743	0.595	0.421	0.246	0.095	-0.002
8.0	0.984	0.939	0.864	0.755	0.611	0.439	0.261	0.105	0.003

Table 8.  $K/K_0$  in a line pipe with OD = 20 in.,  $h = 0.344$  in.

$L_0/h$	0.1	0.2	0.3	0.4	0.5	0.6	0.7	0.8	0.9
Outer circumferential crack, $N_\infty=0, M_o=0$									
1.0	0.945	0.817	0.664	0.508	0.366	0.247	0.147	0.074	0.033
2.0	0.967	0.882	0.766	0.628	0.481	0.340	0.210	0.107	0.049
3.0	0.975	0.911	0.816	0.695	0.553	0.405	0.258	0.133	0.06
4.0	0.980	0.927	0.846	0.737	0.603	0.454	0.297	0.156	0.071
5.0	0.983	0.937	0.866	0.767	0.640	0.492	0.329	0.176	0.081
6.0	0.985	0.944	0.879	0.788	0.667	0.522	0.356	0.193	0.090
7.0	0.986	0.948	0.889	0.803	0.688	0.546	0.378	0.209	0.098
8.0	0.987	0.951	0.896	0.815	0.704	0.565	0.396	0.222	0.105
Outer circumferential crack, $N_\infty=0, M_o \neq 0$									
1.0	0.944	0.805	0.627	0.443	0.273	0.134	0.040	-0.011	-0.034
2.0	0.966	0.874	0.741	0.580	0.407	0.242	0.110	0.021	-0.028
3.0	0.975	0.905	0.797	0.657	0.491	0.318	0.164	0.048	-0.020
4.0	0.980	0.922	0.830	0.705	0.549	0.376	0.209	0.073	-0.011
5.0	0.982	0.933	0.852	0.738	0.591	0.419	0.245	0.095	-0.002
6.0	0.984	0.940	0.867	0.762	0.622	0.454	0.276	0.114	0.006
7.0	0.986	0.945	0.877	0.779	0.645	0.480	0.300	0.131	0.014
8.0	0.986	0.948	0.884	0.791	0.663	0.501	0.320	0.145	0.022
Inner circumferential crack, $N_\infty=0, M_o=0$									
1.0	0.944	0.814	0.659	0.503	0.360	0.243	0.145	0.073	0.033
2.0	0.965	0.876	0.754	0.613	0.465	0.326	0.200	0.102	0.048
3.0	0.973	0.903	0.801	0.672	0.527	0.380	0.240	0.124	0.058
4.0	0.978	0.918	0.828	0.709	0.569	0.419	0.269	0.141	0.067
5.0	0.980	0.927	0.845	0.735	0.599	0.448	0.292	0.155	0.074
6.0	0.982	0.933	0.857	0.753	0.621	0.471	0.312	0.167	0.080
7.0	0.983	0.938	0.866	0.766	0.638	0.490	0.327	0.177	0.086
8.0	0.984	0.941	0.873	0.777	0.652	0.505	0.341	0.186	0.092
Inner circumferential crack, $N_\infty=0, M_o \neq 0$									
1.0	0.942	0.801	0.620	0.435	0.266	0.128	0.037	-0.013	-0.034
2.0	0.964	0.867	0.728	0.562	0.387	0.224	0.098	0.015	-0.030
3.0	0.972	0.896	0.779	0.629	0.459	0.287	0.141	0.036	-0.024
4.0	0.977	0.912	0.809	0.672	0.507	0.332	0.174	0.054	-0.018
5.0	0.980	0.922	0.828	0.700	0.541	0.366	0.200	0.068	-0.012
6.0	0.981	0.928	0.841	0.720	0.566	0.392	0.222	0.081	-0.007
7.0	0.983	0.933	0.851	0.735	0.586	0.412	0.239	0.092	-0.001
8.0	0.984	0.936	0.858	0.747	0.601	0.429	0.254	0.102	0.004

shell theory and three dimensional finite element results given in Ref. 18. The agreement appears to be quite satisfactory.

The normalizing stress intensity factor  $K_0$  which appears in the tables is the corresponding plane strain value for an edge-cracked plate of thickness  $h$  and crack depth  $L_0$  and is given by

$$K_0 = K_{ot} = \frac{N_\infty}{h} \sqrt{h} g_t(L_0/h),$$

$$g_t(\xi) = \sqrt{\pi} \xi (1.1216 + 6.5200\xi^2 - 12.3877\xi^4 + 89.0554\xi^6 - 188.6080\xi^8 + 207.3870\xi^{10} - 32.0524\xi^{12}),$$

$$\xi = L_0/h, \quad (7)$$

for membrane loading, and

$$K_0 = K_{ob} = \frac{6M_\infty}{h^2} \sqrt{h} g_b(L_0/h),$$

$$g_b(\xi) = \sqrt{\pi} \xi (1.1202 - 1.8872\xi + 18.0143\xi^2 - 87.3851\xi^3 + 241.9124\xi^4 - 319.9402\xi^5 + 168.0105\xi^6), \xi = L_0/h \quad (8)$$

for (local) bending.

Tables 1 to 8 give the Mode I stress intensity factor at the maximum penetration point  $L = L_0$  of a semi-elliptical surface crack defined by

$$\frac{L^2}{L_0^2} + \frac{X_2^2}{a^2} = 1; \text{ or } L = L_0 \sin \phi, X_2 = a \cos \phi. \quad (9)$$

The stress intensity factor at other locations along the crack front may be obtained by using the following approximate formula:

$$K(\phi) = K\left(\frac{\pi}{2}\right) \left[ 1 - (1 + \cos 2\phi) \left( 0.2323 - 0.0615 \frac{L_0}{h} \right) \right], \quad (10)$$

where  $K(\pi/2)$  is given by Tables 1-8.

If the stress state in the crack region is not "uniform," it may be decomposed into appropriate membrane and bending resultants which are functions of  $X_2$ . For example, in the case of gross bending  $M_o$ , the local resultants are given by Eqs. 5 and 6. In this case, too, since generally  $X_2^2 \ll 2R^2$ , the stress intensity factors may be approximated by the uniform loading results given in the tables by assuming that  $N_\infty = M_o R h / I$  and  $M_\infty = M_o h^3 / 12I$ . Some sample results showing the effect of curvature (i.e., of the term involving  $X_2^2 / 2R^2$  in Eqs. 5 and 6) in the case of gross bending are given in Table 9. In this table, too, the respective normalizing stress intensity factors are given by Eqs. 7 and 8. Note that for the pipe dimensions under consideration the results are three to four orders of magnitude smaller than the corresponding stress intensity factors under uniform loading.

## 2.2 Stress Intensity Factors for a Through Crack

If the geometry of the cracked shell or the external

Table 9. The stress intensity factor ratio  $10^4(K/K_0)$  at the deepest penetration point of a semi-elliptic outer circumferential crack in a pipe subjected to parabolic loadings.  $OD = 20$  in.,  $h = 0.344$  in.,  $\nu = 0.3$ .

$N_{11} = M_0 X_2^2 / 2R^2, M_{11} = 0$										
$a/h$	$L_0/h$	0.1	0.2	0.3	0.4	0.5	0.6	0.7	0.8	0.9
1.0		0.024	0.062	0.080	0.078	0.063	0.043	0.026	.012	0.004
1.5		0.032	0.089	0.129	0.138	0.121	0.089	0.055	0.026	0.010
2.0		0.083	0.247	0.379	0.432	0.400	0.311	0.200	0.096	0.035
2.5		0.175	0.538	0.863	1.032	1.003	0.813	0.542	0.271	0.097
3.0		0.320	1.006	0.673	2.077	2.098	1.764	1.217	0.625	0.227
3.5		0.529	1.699	2.896	3.711	3.875	3.366	2.396	1.263	0.467
4.0		0.810	2.645	4.616	6.076	6.530	5.843	4.277	2.312	0.875
4.5		1.169	3.882	6.904	9.302	10.261	9.429	7.088	3.928	1.526
5.0		1.618	5.429	9.822	13.514	15.254	14.366	11.064	6.281	2.512

$N_{11} = 0, M_{11} = M_0 X_2^2 / 2R^2$										
$a/h$	$L_0/h$	0.1	0.2	0.3	0.4	0.5	0.6	0.7	0.8	0.9
1.0		0.025	0.069	0.097	0.098	0.082	0.057	0.032	0.013	.002
1.5		0.033	0.100	0.154	0.173	0.157	0.119	0.072	0.031	0.066
2.0		0.127	0.402	0.659	0.786	0.756	0.604	0.385	0.175	0.043
2.5		0.184	0.602	1.032	1.290	1.300	1.082	0.723	0.344	0.093
3.0		0.336	1.129	1.997	2.591	2.715	2.358	1.628	0.805	0.236
3.5		0.555	1.899	3.453	4.620	5.003	4.491	3.207	1.641	0.518
4.0		0.850	2.956	5.495	7.547	8.410	7.780	5.724	3.026	1.015
4.5		1.229	4.333	8.205	11.531	13.182	12.521	9.468	5.154	1.828
5.0		1.698	6.053	11.653	16.709	19.540	19.020	14.751	8.251	3.077

loads are not properly symmetric, then Mode II and Mode III components of the stress intensity factor would no longer be zero. Furthermore, in this case the crack initiation (for example, under cyclic loading) would be in a plane other than meridional or circumferential. The problem may be important in spirally welded line pipes having weld defects. The solution of such problems requires the formulation of the most general crack problem in cylindrical shells, namely that of an arbitrarily oriented crack under general non-symmetric loading conditions. The solution of this problem and extensive results for a through crack are given in Ref. 25. Again, selecting the local coordinate system as in Fig. 21, for a spirally oriented crack which occupies  $X_1 = 0, -a < X_2 < a, -h/2 < X_3 < h/2$  the Modes I, II, and III stress intensity factors around the crack tip  $X_2 = a$  may be defined as follows:

$$K_I(X_3) = \lim_{X_2 \rightarrow a} [2\pi(X_2 - a)]^{1/2} \sigma_{11}(0, X_2, X_3), \quad (11)$$

$$K_{II}(X_3) = \lim_{X_2 \rightarrow a} [2\pi(X_2 - a)]^{1/2} \sigma_{12}(0, X_2, X_3), \quad (12)$$

$$K_{III}(X_3) = \lim_{X_2 \rightarrow a} [2\pi(X_2 - a)]^{1/2} \sigma_{13}(0, X_2, X_3), \quad (13)$$

where  $\sigma_{ij}, (i, j = 1, 2, 3)$  are the stress components referred to  $X_1, X_2, X_3$  coordinates (see Figs. 2 and 21 for the coordinate system).

In the shell analysis the external loads are given in terms of stress and bending resultants. Therefore, the problem may be solved more conveniently by assuming only one of the five resultants to be nonzero at a time. The general solution may then be obtained by a suitable superposition. As in the symmetric case, there is one stress intensity factor associated with each of the five resultants. The stress component corresponding to the

membrane, bending, and transverse shear resultants which may be applied to the cylinder along the crack are given by

$$\begin{aligned} \sigma_m &= N_{11}/h, \sigma_b = 6M_{11}/h^2, \sigma_s = N_{12}/h, \\ \sigma_t &= 6M_{12}/h^2, \sigma_v = (3/2)V_1/h. \end{aligned} \quad (14)$$

The nominal stresses defined by Eq. 14 will be designated as "membrane," "bending," in-plane "shear," "twisting," and "transverse shear," and  $N_{11}, M_{11}, N_{12}, M_{12},$  and  $V_1$  are (a measure or amplitude of) the corresponding crack surface loading.

Some sample results for a pipe which contains a through crack along a  $45^\circ$  spiral and which is subjected to torsion are given in Table 10. In this case the membrane resultant  $N_{11}$  is the only nonzero load component. However, because of the lack of geometric symmetry none of the other stress intensity components vanishes. The normalized stress intensity factors  $k_{im}, (i = m, b, s, t, v)$  given in the table are related to the Modes I, II, and III stress intensity factors at the crack front as follows:

$$\begin{aligned} k_{mm} &= K_I(0)/\sigma_m \sqrt{\pi a}, \\ k_{bm} &= [K_I(h/2) - K_I(0)]/\sigma_m \sqrt{\pi a}, \\ k_{sm} &= K_{II}(0)/\sigma_m \sqrt{\pi a}, \\ k_{tm} &= [K_{II}(h/2) - K_{II}(0)]/\sigma_m \sqrt{\pi a}, \\ k_{vm} &= K_{III}(0)/\sigma_m \sqrt{\pi a}, \sigma_m = N_{11}/h, \end{aligned} \quad (15)$$

where  $h, 2a,$  and  $R$  are again the thickness, the crack length and the mean radius. Needless to say, in this inplane membrane loading  $K_I$  is the dominant stress intensity factor; the components  $k_{im}, (i = b, s, t, v)$  represent the coupling effects. Note that as  $R \rightarrow \infty$  the problem reduces to that of a flat plate,  $k_{mm}$  becomes 1 and the remaining stress intensity components vanish.

In the special case of a circumferential through crack shown in Fig. 2, if the loading is symmetric with respect to the plane of the crack, then  $K_{II}$  and  $K_{III}$  would be zero. For this practical case the membrane and bending components of stress intensity factors for a cylinder under uniform tension  $N_{11}$  (or gross bending  $M_0$ ) are given in Figs. 3 and 4. In these figures the shell parameter  $\lambda_2$  is defined by (see Fig. 2)

$$\lambda_2 = [12(1 - \nu^2)]^{1/4} a / \sqrt{Rh}. \quad (16)$$

Similarly, if the cylinder is subjected to local bending so that in the corresponding perturbation problem the symmetric bending moment  $M_{11}$  applied to the crack surfaces is the only nonzero external load, then the primary and coupling stress intensity factors may be defined as

$$\begin{aligned} k_{bb} &= [K_I(h/2) - K_I(0)]/\sigma_b \sqrt{\pi a}, \\ k_{mb} &= K_I(0)/\sigma_b \sqrt{\pi a} \end{aligned} \quad (17)$$

where  $\sigma_b$  is given by Eq. 14. For the crack geometry shown in Fig. 2 the results are given in Figs. 5 and 6.

Table 10. Stress intensity factor ratios in an isotropic cylindrical shell containing an inclined crack under uniform membrane loading  $N_{11}$ ,  $\nu = 0.3$ ,  $\beta = 45^\circ$ .

	$h/R$	$a/h$				
		1	2	3	5	10
$k_{mm}$	1/5	1.097	1.302	1.544	2.030	3.486
	1/10	1.049	1.167	1.321	1.665	2.516
	1/15	1.033	1.116	1.230	1.501	2.199
	1/25	1.020	1.072	1.148	1.341	1.886
	1/50	1.010	1.037	1.079	1.194	1.563
	1/100	1.005	1.019	1.041	1.106	1.337
$k_{bm}$	1/200	1.002	1.010	1.021	1.056	1.192
	1/5	0.084	0.122	0.100	-0.069	-0.761
	1/10	0.058	0.108	0.126	0.079	-0.299
	1/15	0.046	0.093	0.121	0.118	-0.125
	1/25	0.032	0.073	0.104	0.132	0.023
	1/50	0.020	0.049	0.076	0.117	0.120
$k_{sm}$	1/100	0.012	0.031	0.051	0.089	0.139
	1/200	0.007	0.019	0.033	0.062	0.120
	1/5	-0.036	-0.108	-0.190	-0.333	-0.517
	1/10	-0.018	-0.060	-0.113	-0.227	-0.424
	1/15	-0.012	-0.041	-0.081	-0.173	-0.365
	1/25	-0.007	-0.025	-0.052	-0.119	-0.289
$k_{tm}$	1/50	-0.004	-0.013	-0.028	-0.068	-0.192
	1/100	-0.002	-0.007	-0.014	-0.037	-0.117
	1/200	-0.001	-0.003	-0.007	-0.019	-0.067
	1/5	0.012	-0.029	-0.119	-0.432	-4.232
	1/10	0.010	-0.008	-0.053	-0.219	-1.853
	1/15	0.008	-0.002	-0.031	-0.144	-1.244
$k_{vm}$	1/25	0.006	0.002	-0.015	-0.082	-0.757
	1/50	0.004	0.003	-0.004	-0.036	-0.379
	1/100	0.003	0.003	0.000	-0.015	-0.186
	1/200	0.002	0.002	0.001	-0.006	-0.090
	1/5	-0.051	-0.139	-0.261	-0.609	-2.630
	1/10	-0.026	-0.070	-0.131	-0.302	-1.117
	1/15	-0.018	-0.047	-0.088	-0.201	-0.736
	1/25	-0.011	-0.029	-0.053	-0.121	-0.441
	1/50	-0.005	-0.015	-0.028	-0.062	-0.221
	1/100	-0.003	-0.008	-0.014	-0.032	-0.111
	1/200	-0.001	-0.004	-0.008	-0.017	-0.056

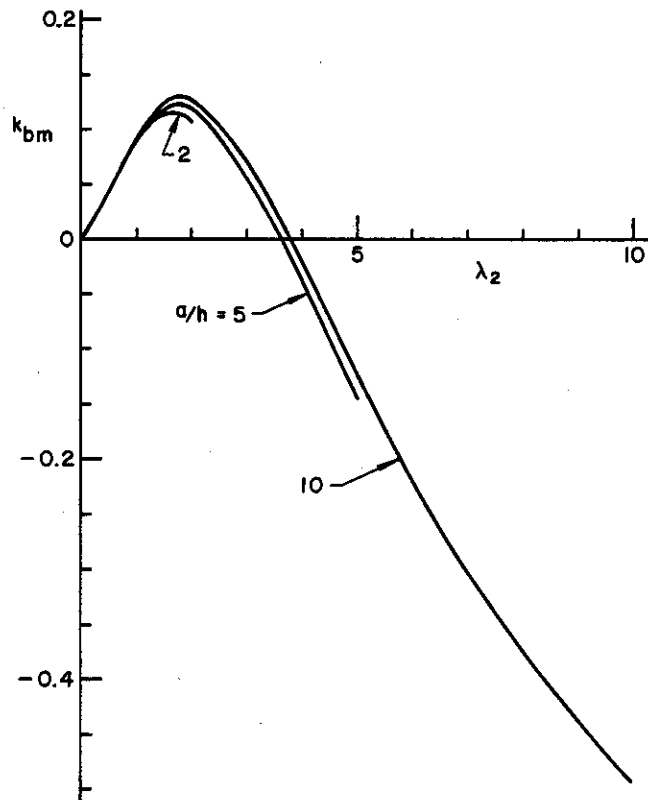


Fig. 4—Bending component of the stress intensity ratio for a circumferentially cracked cylinder under uniform membrane loading ( $N_{11} \neq 0$ ,  $M_{11} = 0$ )

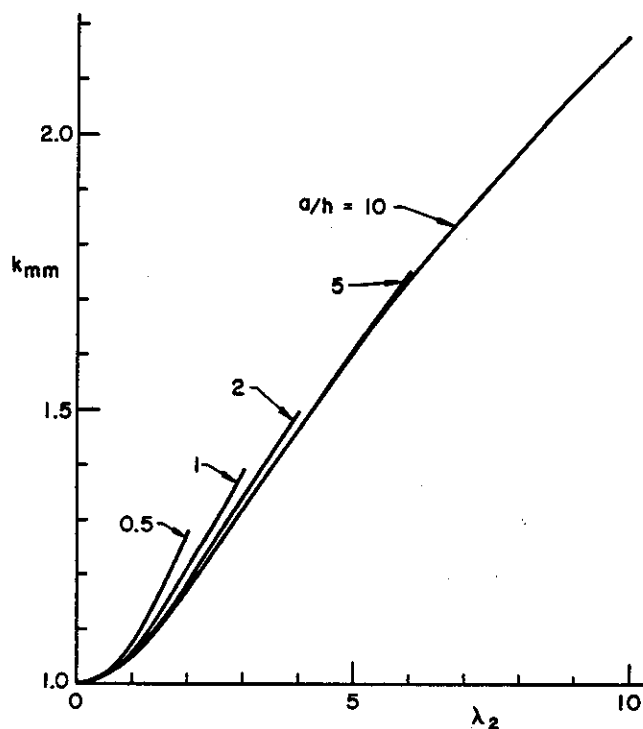


Fig. 3—Membrane component of the stress intensity ratio for a circumferentially cracked cylinder under uniform membrane loading ( $N_{11} \neq 0$ ,  $M_{11} = 0$ )

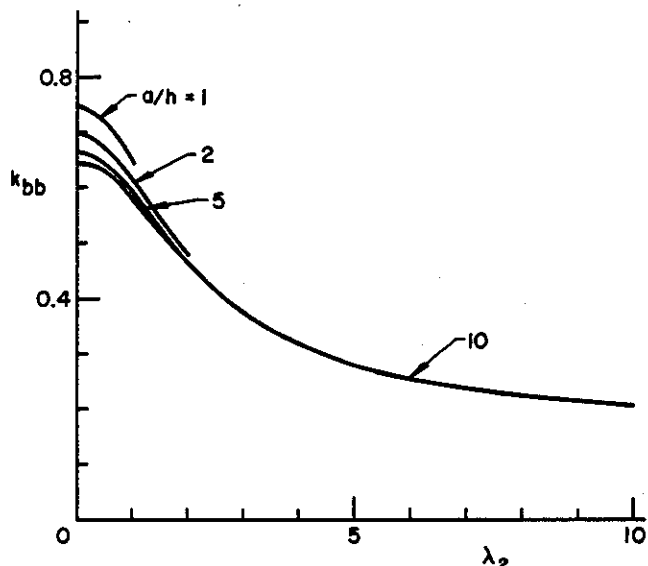


Fig. 5—Bending component of the stress intensity ratio for a circumferentially cracked cylinder under uniform crack surface bending moment ( $N_{11} = 0$ ,  $M_{11} \neq 0$ )

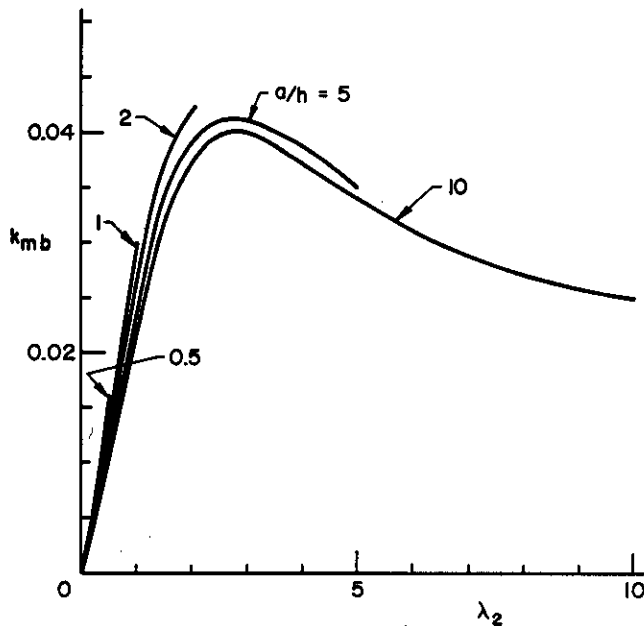


Fig. 6—Membrane component of the stress intensity ratio for a circumferentially cracked cylinder under uniform crack surface bending moment ( $N_{11} = 0$ ,  $M_{11} \neq 0$ )

### 3. Crack Opening Displacement

If the crack in the cylinder wall is relatively deep and long, the material is not brittle and the external loads are sufficiently high, then there may be extensive plastic deformations around the crack region. In this case unlike the  $J$ -controlled predominantly plane strain type contained plastic deformation problems, in the modeling and analysis of the related ductile fracture process the crack-structure geometry and the global mechanics of the phenomenon would be expected to play a major role. For the initiation of ductile fracture some local deformation or strength parameter at the crack front must reach a critical condition. On the other hand, for the subsequent stable or unstable crack growth the global energy balance condition must be satisfied. Clearly, the phenomenon in shells is far too complex for a single parameter characterization. However, for the purpose of analyzing and correlating the experimental results an appropriate single fracture mechanics parameter has obvious advantages. Among the required features of such a parameter one may mention the following: (a) The parameter must be sufficiently representative of the intensity of the local deformation state, (b) its theoretical evaluation must be relatively insensitive to the accuracy of the continuum modeling of the related elastic-plastic crack problem, (c) the corresponding mechanics problem should be analytically tractable and (d) it must be a relatively simple and accurately measurable quantity.

In our view, for the shell problem the crack opening displacement (COD) seems to come closest fulfilling these requirements. Whatever the actual mechanics of the fracture process, the intensity of local deformations

may be looked upon as an acceptable measure of the fracture resistance as well as the intensity of the applied loads. COD is certainly a reasonably good representative of the local deformation state and can be measured accurately. At the same time it is a global quantity in the sense that it represents the integrated effects of the inelastic deformations in the crack region. Thus, it may be assumed that the calculated value of COD would not be as sensitive as some other fracture parameters to the details of the elastic-plastic modeling of the part-through crack problem in shells.

The continuum plasticity problem for the shells appears to be analytically intractable. In this study a modified version of the standard plastic strip model will be used to model the problem. This is nothing but a fully-plastic line spring model. In the model it is assumed that the net ligament and a certain region around the crack is fully yielded, with the size  $p$  of the yield zones as well as the membrane and the bending resultants  $N$  and  $M$  in the yield zones being unknown. In the formulation of the shell problem these three additional unknowns are accounted for by the conditions that the membranes and bending components of the stress intensity factor be zero at  $X_2 = \mp(a + p)$  and  $N$  and  $M$  satisfy a yield condition, namely

$$K_m(a + p) = 0, \quad (18)$$

$$K_b(a + p) = 0, \quad (19)$$

$$\frac{N}{h\sigma_F} + \frac{|M|}{h^2\sigma_F} = 1 \quad (20)$$

where  $\sigma_F$  is the "flow stress" of the material.

In the particular formulation of the shell problem such as that described in Ref. 21, the calculated quantities are the crack surface displacement  $u_1(0, X_2)$  and the crack surface rotation  $\beta_1(0, X_2)$  at the neutral surface. Thus, in the symmetric problem under consideration, the crack opening displacement at any point  $(0, X_2, X_3)$  on the crack surface may easily be obtained from

$$\delta(X_2, X_3) = 2u_1(+0, X_2) + 2X_3\beta_1(+0, X_2), \quad \left(-a < X_2 < a, -\frac{h}{2} < X_3 < \frac{h}{2}\right). \quad (21)$$

Some sample results giving the crack mouth opening displacement

$$\text{COD} = \delta(0, h/2) \quad (22)$$

for a 30-inch (outer) diameter line pipe are shown in Figs. 7–10. In these calculations the cylinder is assumed to be under a uniform axial stress  $\sigma_o$ . The notation for the dimensions of the pipe and the surface crack are shown in Fig. 21,  $E$  is the Young's modulus, and  $\sigma_F$  is the flow stress. Note that the results are in dimensionless form. Similar results for the other standard line pipe dimensions are given in Ref. 24.

From the figures one may observe that for small values of the stress ratio  $\sigma_o/\sigma_F$ , COD is a linear function of the external load which corresponds to the linear

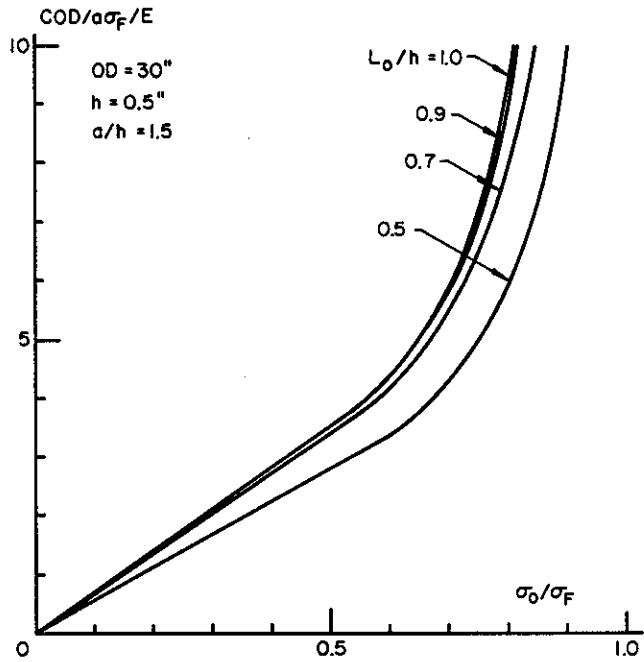


Fig. 7—COD vs.  $\sigma_o/\sigma_F$  for a 30-in. diameter pipe

elastic response of the cracked shell. For greater values of  $\sigma_o/\sigma_F$  as expected the relationship is severely non-linear and, for given crack and shell dimensions, at a certain value of the stress ratio COD behaves nearly in an asymptotic manner. From the viewpoint of the mechanics of the problem this behavior may be interpreted as some kind of instability phenomenon.

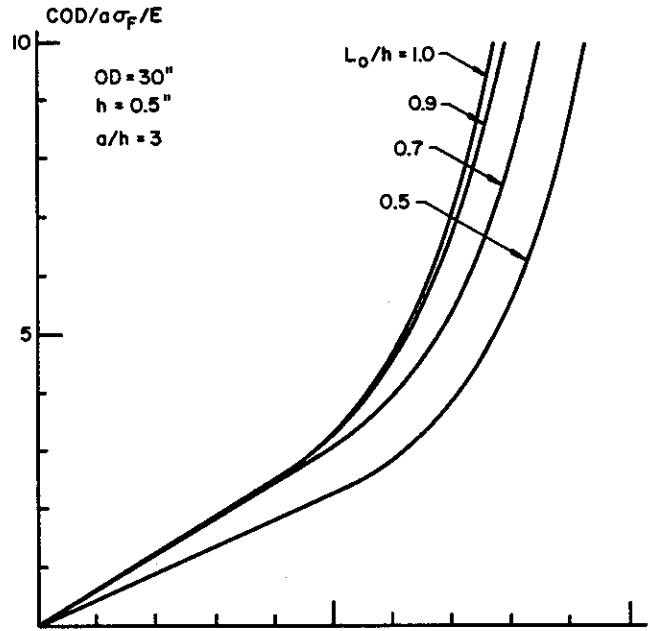


Fig. 9—COD vs.  $\sigma_o/\sigma_F$  for a 30-in. diameter pipe

#### 4. The Pipe Experiments

The experimental work on a 20-inch line pipe was undertaken primarily to verify the validity of some of the analytically obtained elastic and elastic-plastic results for a part-through circumferential crack and to perform crack morphology studies. The pipe was tested under four-point bending. The dimensions of the pipe and the locations of the loading pads and the crack are shown in Fig. 11.

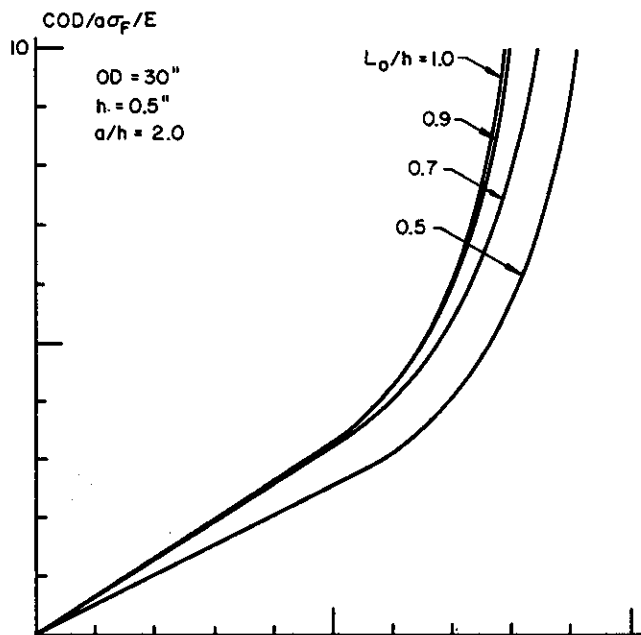


Fig. 8—COD vs.  $\sigma_o/\sigma_F$  for a 30-in. diameter pipe

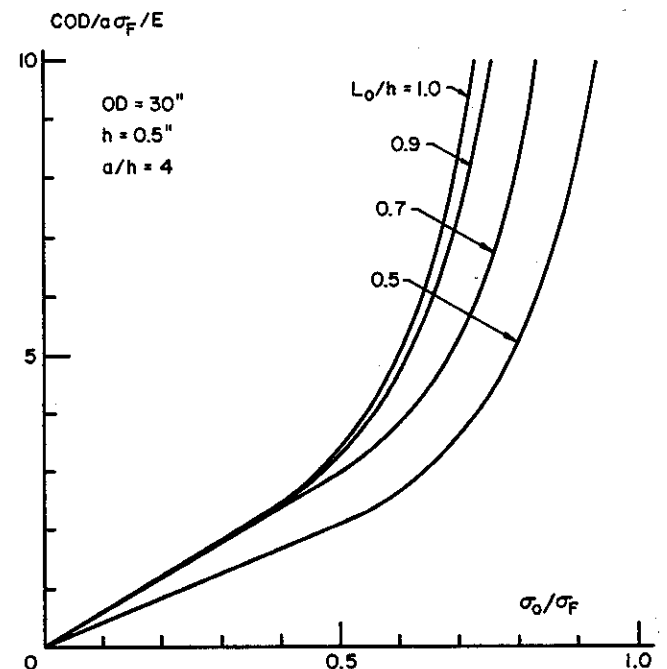


Fig. 10—COD vs.  $\sigma_o/\sigma_F$  for a 30-in. diameter pipe

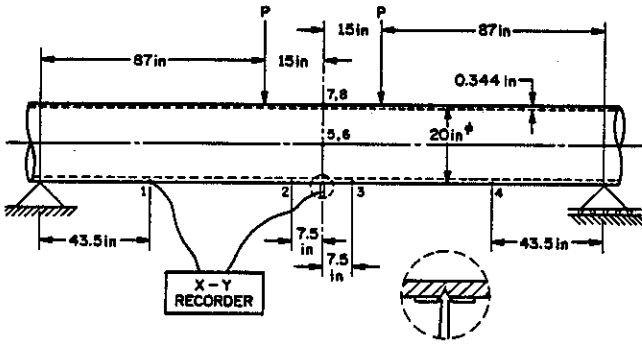


Fig. 11—The geometry and dimensions of the pipe specimens

#### 4.1 Stresses in a Pipe under “Four-Point” Bending

In solving the crack problems in pipes it was indicated that for a given loading condition the stresses in the pipe without the crack are known. The crack problem was then solved under self-equilibrating loads applied to the crack surfaces only. In the problem under consideration the pipe is under “four-point” bending (Fig. 1). Generally in such problems it is assumed that the pipe is subjected to gross bending and the stresses may be obtained by treating it as a “beam.” However, in most cases, it is necessary to verify the results given by the beam theory by carrying out a somewhat more realistic stress analysis of the pipe and by considering the details of the loading fixtures.

At the four points shown in Fig. 11 the loads were applied to the pipe by 6-in. wide semicircular saddles. To prevent a possible collapse of the pipe wooden blocks of 4 in.  $\times$  4 in. cross-section were inserted into the pipe at the load locations (Fig. 12). Other relevant dimensions are shown in Fig. 11.

A shell theory was used to calculate the stresses in the pipe. (KSHEL developed by Professor A. Kalnins at Lehigh University.) This is a numerical technique in which all field quantities including the external loads are expanded into Fourier series in  $\theta$  and a segmental integration is used in the axial direction. The shell equations are expressed in terms of a system of first order differential equations. The resulting “two-point boundary value problem” is then solved by reducing it to an initial value type problem. In order to avoid a highly complicated contact problem, the form of the “contact” stresses at the locations of the loads was assumed beforehand (see Fig. 12). Following were the main assumptions: (a) the contact at all locations is frictionless, (b) the pressure distribution under the saddles is independent of the axial coordinate and has a cosine distribution in  $\theta$ , and (c) the pressure distribution between the wooden blocks and the shell is uniform. Thus, the transverse load  $N(\theta)$  applied to the pipe would be of the form shown in Fig. 12, where  $N(\theta) = N_o \cos \theta$ ,  $N_1$  is unknown, and  $\theta_1 = c/2R \approx 0.2$  rad.,  $c = 4$  in. being the width of the wooden block. From the equilibrium condition  $N_o$  is found to be

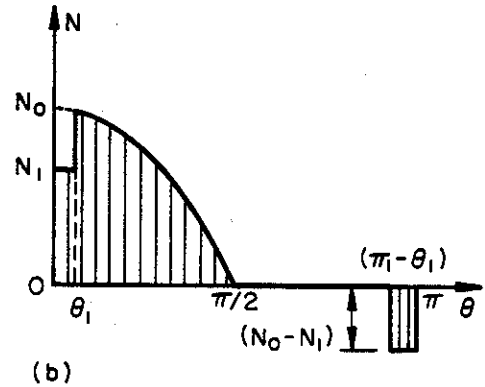
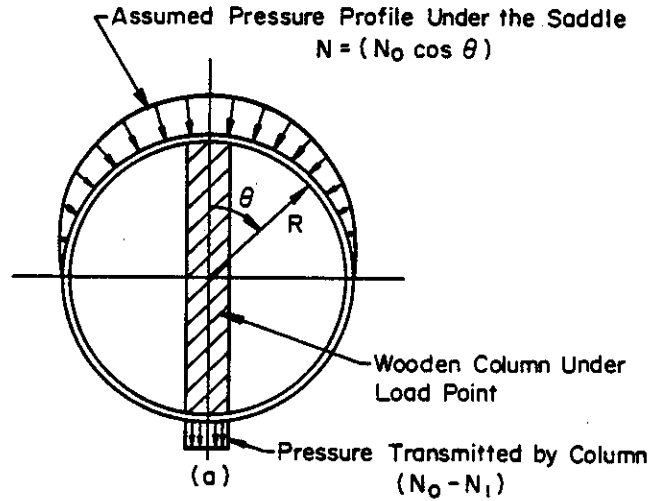


Fig. 12—Assumed distribution of the applied load through the saddles and the wooden blocks in the pipe specimens

$$\int_{-\pi/2}^{\pi/2} N(\theta) \cos \theta R d\theta = P, N_o = 2P/\pi R. \quad (23)$$

The load  $N_1$  is determined from the following displacement compatibility condition:

$$W(0) + W(\pi) = \frac{\sigma_w l_w}{E_w}, \quad (24)$$

where  $W(\theta)$  is the radial displacement in the shell (positive if outward),  $\sigma_w$  is the stress in and  $l_w$  and  $E_w$  are the length and the Young’s modulus of the wooden block.

In the analysis the loading condition shown in Fig. 12 is used only in the interior load locations  $x = \pm 15$  in. (Fig. 11). For simplicity the pipe ends were assumed to be “simply-supported,” that is, at  $x = \pm 102$  in. it was assumed that

$$(N_{\phi\phi}, M_{\phi\phi}, N_{\phi\theta}, W) = 0, \quad (25)$$

where  $\phi$  and  $\theta$  are respectively the axial and the circumferential coordinates and  $N_{ij}$  and  $M_{ij}$  ( $i, j = \phi, \theta$ ) are the membrane and bending resultants.

Some calculated results for the dimensions shown in Fig. 11 are given in Figs. 13–15. Fig. 13 shows the  $\theta$ -distribution of the circumferential stress  $\sigma_{\theta\theta}$  and the axial stresses  $\sigma_{xi}$  and  $\sigma_{xo}$  in the pipe at the plane of

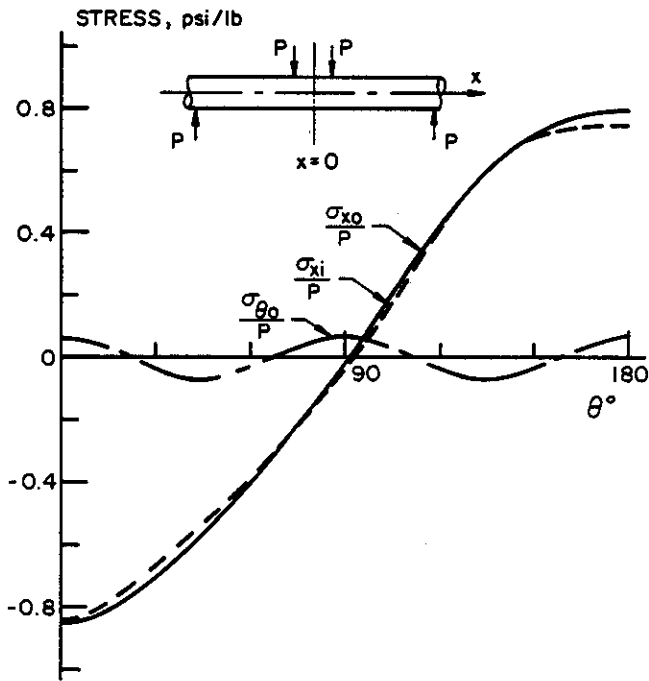


Fig. 13—Circumferential variation of the hoop ( $\sigma_{\theta o}$ ) and the axial stresses ( $\sigma_{xi}, \sigma_{xo}$ ) at  $x = 0$  plane in the pipe under "four-point bending"

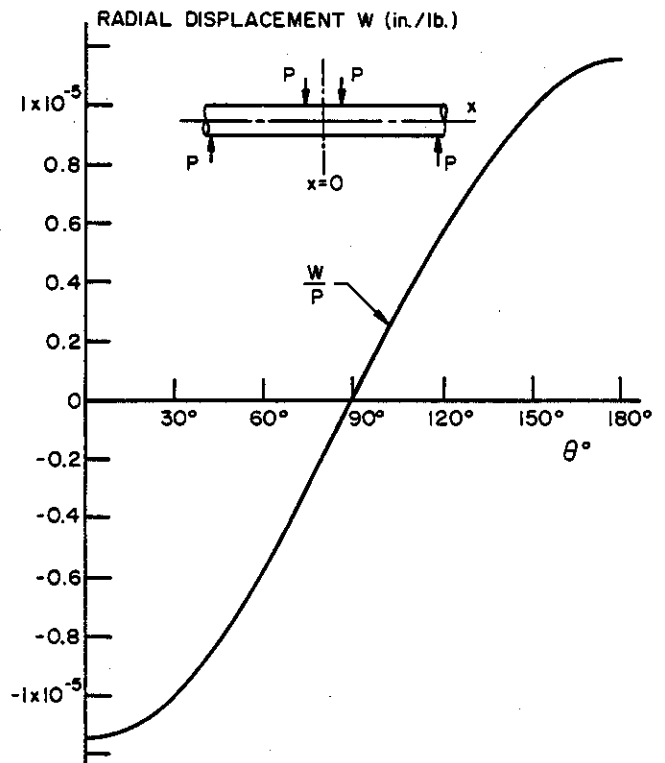


Fig. 15—The circumferential variation of the radial displacement  $W$  at  $x = 0$  plane

symmetry  $x = 0$  where the subscripts  $o$  and  $i$  stand for points on the "outer" and the "inner" surface of the shell, respectively.  $\sigma_{xo} \neq \sigma_{xi}$  implies local bending of the shell wall; that is,

$$(\sigma_{xo} + \sigma_{xi})/2 = N_{\phi\phi}/h, (\sigma_{xo} - \sigma_{xi})/2 = 6M_{\phi\phi}/h^2. \quad (26)$$

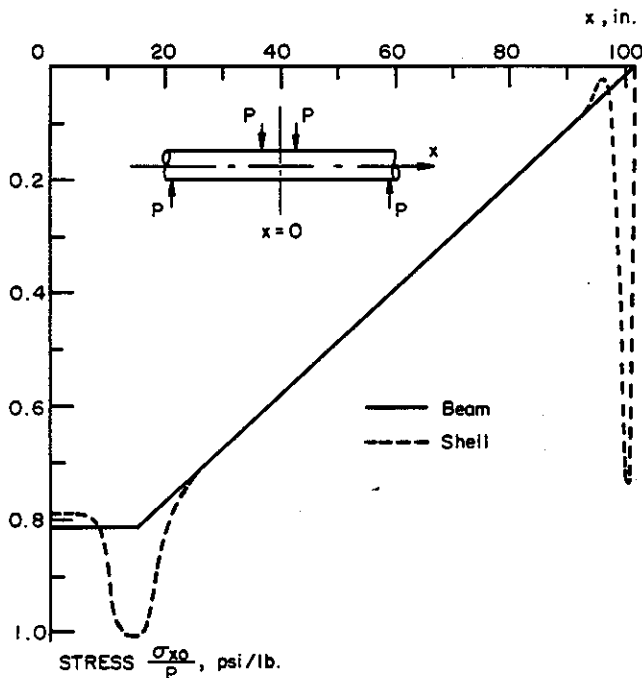


Fig. 14—Variation of the maximum axial stress ( $\sigma_{xo}$  at  $\theta = \pi$ ) along the pipe

Fig. 14 shows the distribution of the axial stress  $\sigma_{xo}$  at  $\theta = \pi$  as a function of  $x$ . The figure also shows the same stress component obtained from the beam theory. From Fig. 13 it may be observed that the local bending due to the variation of the membrane stress  $\sigma_x$  in thickness direction at the location of the crack (i.e.,  $x = 0, \theta = \pi$ ) is not very significant (the maximum bending stress  $\sigma_b = 6M_{\phi\phi}/h^2$  is approximately 3.7% of the membrane stress  $\sigma_m = N_{\phi\phi}/h$ ). Similarly, the difference between the stresses at the crack location obtained from the shell and the beam theories is approximately 3.1% of the nominal value (Fig. 14). Therefore, in the pipe under consideration using the beam theory to calculate the stresses would involve no substantial error.

Fig. 15 gives some idea about the ovalization of the pipe at  $x = 0$  plane. In this figure  $W(\theta)$  is the radial component of the displacement (positive if outward). It should be emphasized that the problem was solved for  $P = 1$  by using the actual dimensions of the pipe given in Fig. 11. Thus all quantities shown in Fig. 13–15 are per unit applied load and are not dimensionless.

#### 4.2 Mechanical Properties of the Material

Before testing, specimens were cut from the pipe in the longitudinal direction to obtain simple mechanical properties of the material. A sample result of the tensile tests is shown in Fig. 16. Even though the material was nominally designated as being X60 the yield and ultimate strengths were found to be  $\sigma_{YS} \cong 68$  ksi,  $\sigma_{UL} \cong 82.9$  ksi. Various views of the ruptured tensile specimens

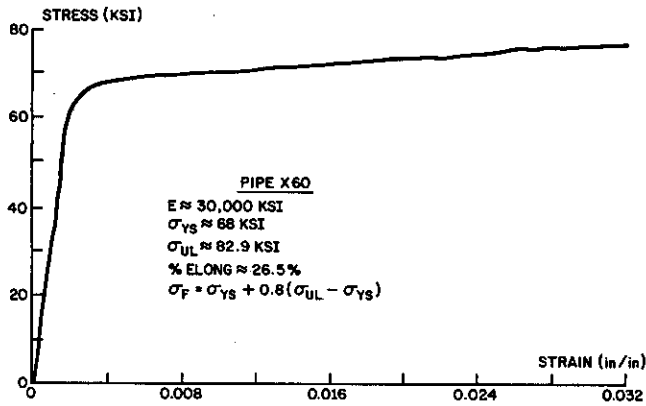


Fig. 16—Mechanical properties of the pipe material, nominally designated as X60, obtained from a tensile specimen cut parallel to the axis of the pipe (i.e. the rolling direction)

and are shown in Fig. 17. The most striking feature of the fracture surfaces was the severe delamination of the material parallel to the pipe surfaces. There was also severe necking in both thickness and circumferential directions before fracture.

Specimens were also cut from the pipe in the longitudinal direction for Charpy V-notch experiments. In

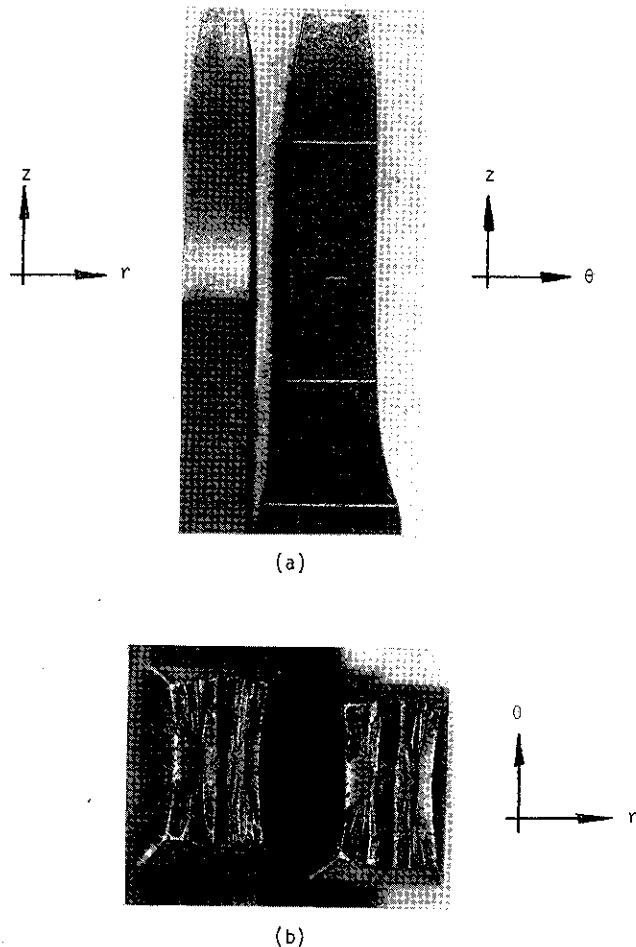


Fig. 17—Various views of the X60 tensile specimen cut from the pipe;  $r$ ,  $\theta$ , and  $z$  refer to the radial, circumferential, and axial directions, respectively

these specimens the notch was cut in the circumferential (or  $\theta$ ) direction (that is, the loads were applied in  $\theta$ - $z$  plane, see Fig. 17). The test results are shown in Fig. 18 where the solid line represents an approximate fit to the data. The results are characteristic of pipeline steels, namely they indicate relatively high toughness, and no distinct shelf values.

#### 4.3 The Fatigue Experiments

The length and load point locations of the pipe specimens shown in Fig. 11 were determined largely to accommodate the capacity of the Amsler hydraulic jacks used for loading the specimens. The machine capacity had to be sufficient to produce a bending moment in the unnotched pipe near the full yield or "hinge" value of the moment. Another consideration was the buckling of the pipe on the compression side. Since premature elastic instability could spoil the entire program, some elementary buckling calculations had to be made. First, the following empirical formula developed for the elastic buckling of thin shells under bending was used to calculate an equivalent critical stress<sup>26</sup>:

$$\sigma_{cr} = \frac{Eh}{R\sqrt{3(1-\nu^2)}} [1 - 0.731(1 - e^{-\phi})],$$

$$\phi = \frac{1}{16} \sqrt{R/h}, \quad (27)$$

where  $\sigma_{cr}$  is the critical stress for elastic buckling initiation,  $R$  the mean radius,  $h$  the thickness, and  $E$ ,  $\nu$  are the elastic constants. For the 20-in. diameter steel pipe under consideration (Eq. 27) gives  $\sigma_{cr} \approx 500$  ksi indicating no danger of buckling according to (Eq. 27).

A second calculation was made by assuming that the pipe is under axial compression. Following Ref. 27 the critical stress for this case is given by

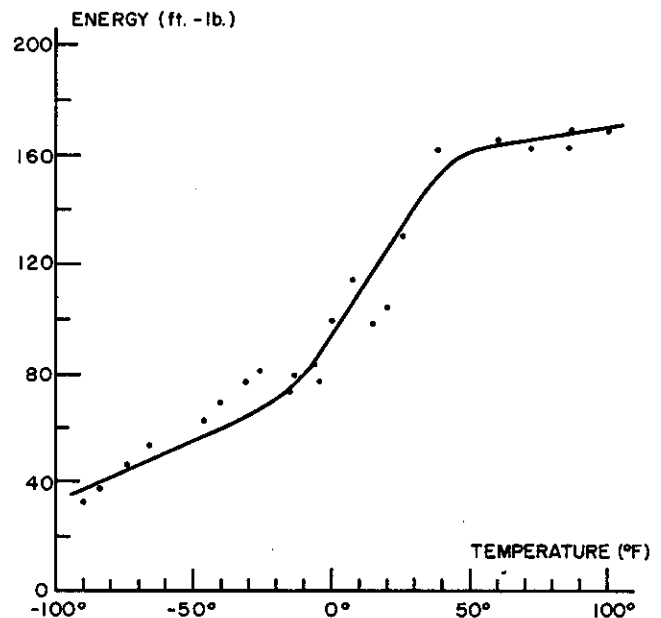


Fig. 18—Results of the Charpy tests for the X60 pipe material

$$\sigma_{cr} = \frac{E \left( \frac{0.6h}{R} - 10^{-7} \frac{R}{h} \right)}{1 + 0.004 \frac{E}{\sigma_{PL}}} \quad (28)$$

where  $\sigma_{PL}$  is the proportionality limit of the material. Equation 28 takes into account initial imperfections (i.e., deviations of the shell surface from an ideal circular cylinder) and assumes that the deflections may not be small. Taking  $\sigma_{PL} = 58$  ksi, Eq. 28 gives  $\sigma_{cr} \approx 205$  ksi.

It then appears that the elastic buckling should not pose a problem in the pipe tests. A circumferential starter notch was introduced to the pipe specimens by using a 1-in. diameter 0.025-in. thick abrasive disk. Two or three overlapping initial cuts were made to have the desired initial flaw size and particularly to create a "chevron" effect to shorten the crack initiation time. The pipe was then placed in the test frame with the crack on the compression side and the notch was subjected to a precompression stress of approximately 75% of the yield strength of the material. The reason for this was to further speed up the crack initiation process. A sketch of the pipe cross-section through the crack plane is shown in Fig. 19.

The objective of the fatigue tests was twofold. The first was to introduce a natural crack to the pipe wall prior to the fracture tests. The second was to collect some fatigue crack propagation data in shells. The programmed loading and crack front marking technique were used to collect the fatigue data. The same hydraulic jacks were used for cyclic (at 250 cpm) and for static loading. The stress intensity factor calculated in

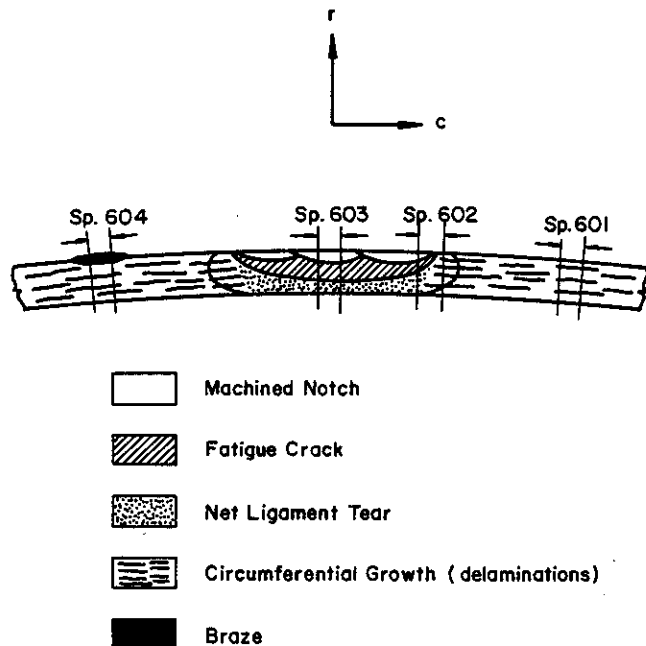


Fig. 19—A sketch of the fracture surface of pipe #6 showing the locations of various specimens used in the scanning electron microscope

Section 2 of this paper was used to correlate the fatigue results. The limited results obtained for the pipes are shown in Fig. 20 superimposed on the results obtained for flat plates with a part-through surface crack and for single edge notched specimens of X-70 steel. The solid line in the figure represents an approximate fit to the air data obtained by Vosikovsky for X70 specimens.<sup>28</sup> All test specimens shown in Fig. 20 had the same crack orientation with respect to the rolling direction of the material. Assuming that the materials X60 and X70 have similar fatigue crack growth characteristics, Fig. 20 shows that the fatigue crack propagation rates in the pipe can be predicted from the data obtained from simple two-dimensional specimens provided the theoretical stress intensity factors for the pipe are available. Conversely, in applications the calculated results such as those given by Tables 1-8 may be used in a simplified fatigue crack growth model obtained from the fatigue characterization of the material (e.g., Fig. 20) to estimate the crack propagation rate.

#### 4.4 Fracture Tests

Following each fatigue experiment the transverse loads  $P$  were slowly increased in order to observe the development of ductile fracture in the pipe (Fig. 11). The fracture tests were carried out by using the same hydraulic jacks and the same load frame as used in the fatigue experiments. Strain gages were mounted at various locations on the specimen to monitor the de-

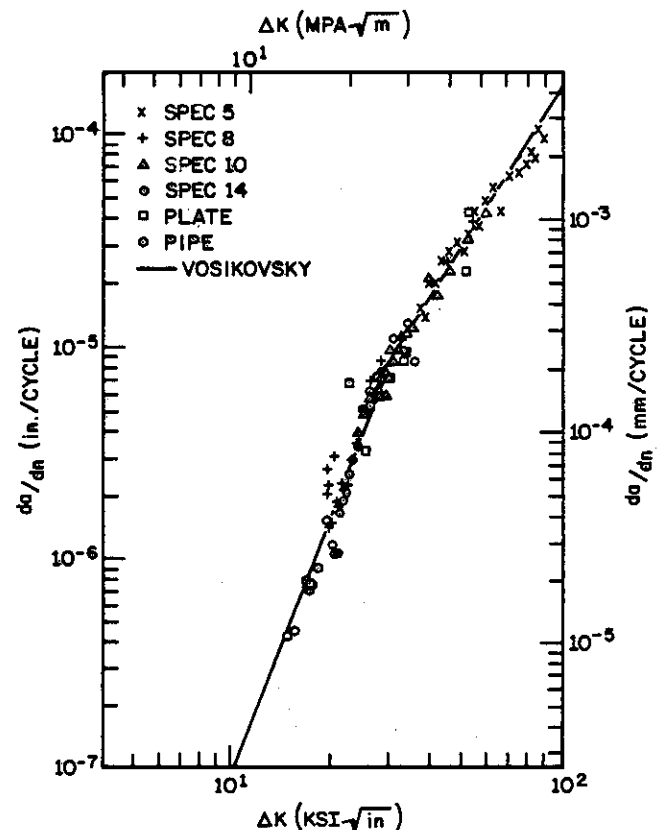


Fig. 20—Fatigue crack propagation in X70 single edge notched and surface cracked plates, and in circumferentially cracked X60 pipes

formations in the pipe and the relative magnitudes of the loads applied by the two jacks. A precalibrated clip gage was used to measure the crack mouth opening displacement. The outputs of gage 1 and the clip gage were connected to an  $x$ - $y$  recorder for continuous recording of the transverse load  $P$  vs. the crack opening displacement COD. An eight channel oscilloscope was used as a back-up to the  $x$ - $y$  recorder and to store the information on a disk. A digital data acquisition system was used to record the outputs from the strain gages at certain values of the load. In order to detect the load level corresponding to the initiation of net ligament rupture, a photo cell was installed inside the pipe opposite the crack, the pipe was darkened by blocking the ends and the light was directed at the crack from outside.

Except for the initial fatigue-sharpening the cracks, the experimental procedure followed and essentially the results found in this study are quite similar to those reported in Ref. 29 by Wilkowski and Eiber. As in Ref. 29, the loading technique used in the present experiments was basically "displacement-controlled." This means that the experimental  $P$  vs. COD curves go through a maximum and then  $P$  starts decreasing as the load point displacement and COD increases. In a "load-controlled" experiment the maximum  $P$  thus attained would have been the fracture instability load.

Altogether six pipes were tested. In two of the pipes the fatigue crack was permitted to propagate through the entire pipe wall. In the remaining four some effort was made to have a part-through fatigue crack of various specific dimensions. The experimentally obtained  $P$  vs. COD curves are shown in Figs. 21-26. Unlike some of the results given in Ref. 29 and except for pipe #2,

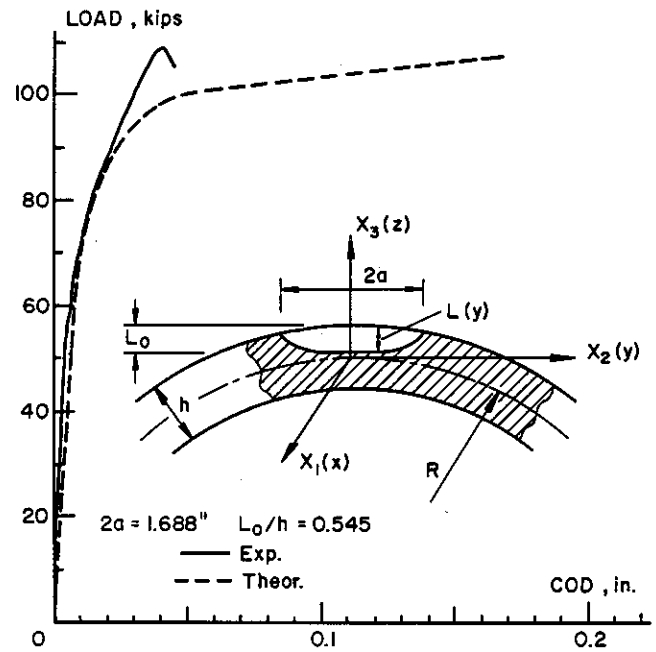


Fig. 22—Transverse load  $P$  vs. COD for pipe # 2

the curves are all "smooth." That is, there were no "kinks" in the curves which would have been an indication of "fracture initiation" or "net ligament rupture." The reason for this is believed to be fatigue sharpening of the crack prior to static loading. Pipe #2 has a relatively short and shallow fatigue crack ( $2a = 1.688$  in.,  $L_0/h = 0.545$ ). In this case the pipe "failed" as a consequence of structural instability (i.e., buckling) rather

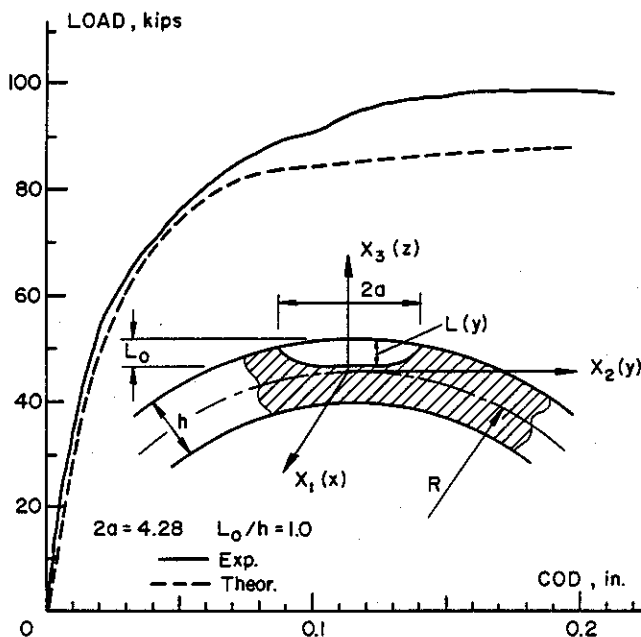


Fig. 21—Transverse load  $P$  vs. COD for pipe # 1

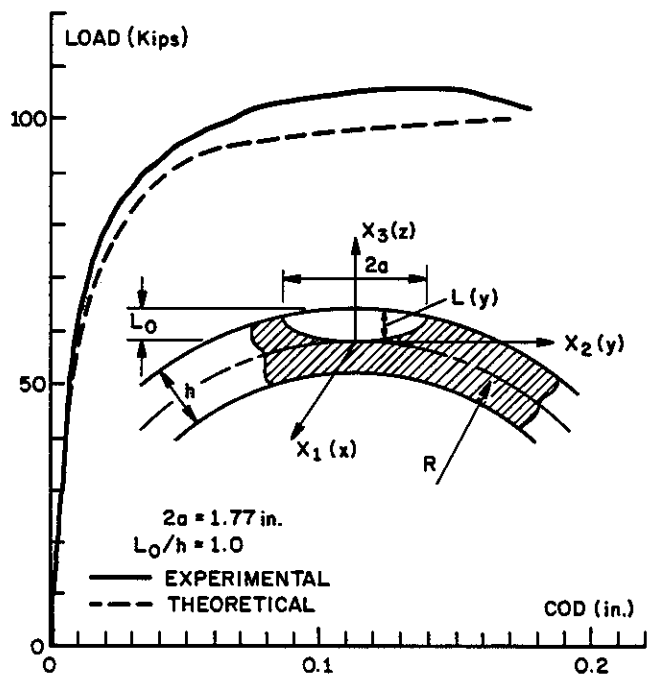


Fig. 23—Transverse load  $P$  vs. COD for pipe # 3

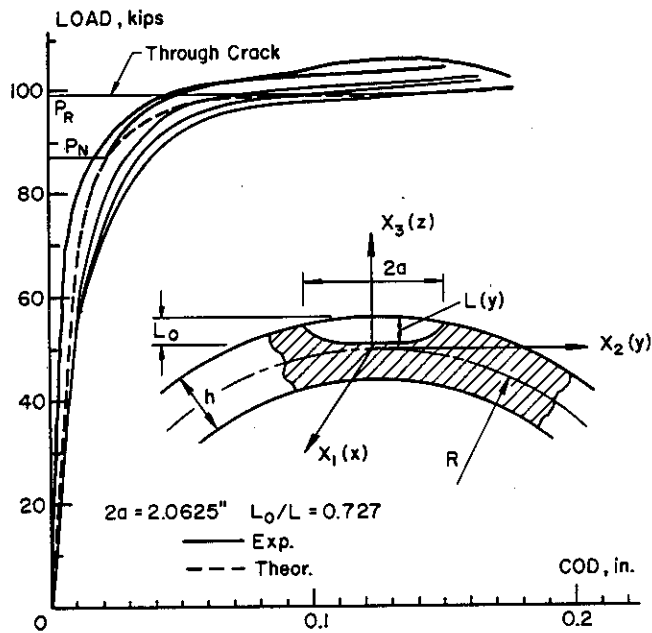


Fig. 24—Transverse load  $P$  vs. COD for pipe # 4

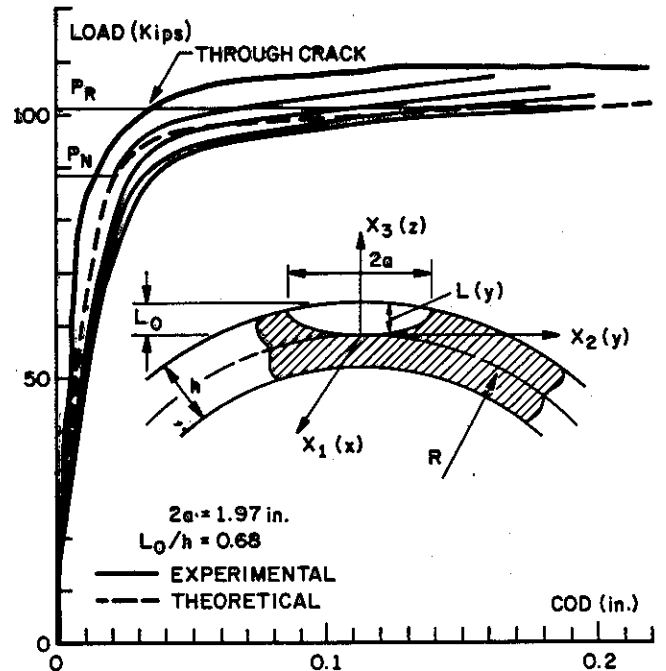


Fig. 26—Transverse load  $P$  vs. COD for pipe # 6

than fracture instability. There was no evidence of crack growth in the pipe wall during the loading process on the test bench. Severe nonlinearity observed in Fig. 22 in the  $P$  vs. COD curve prior to reaching the peak load is an indication of plastic deformations in the crack region, particularly, in the net ligament. The load fell off sharply upon reaching the structural instability value (Fig. 22). The actual development of the buckling of the pipe wall may be seen in Fig. 27.

As pointed out earlier, the elastic instability in the

pipes was not a likely mode of failure, that is, the calculated instability loads were much too high for the material strength to sustain them. However, as seen from Fig. 27, the instability observed in the pipe #2 is inelastic buckling. Even though the peak load in the pipe #6 was the same as that in #2, there was no visible sign of buckling in #6. This may be due to the compliance change in the pipe #6 resulting from the propagation of the through crack on the tension side and, perhaps more likely, to the highly imperfection sensitivity of the buckling process. An important factor in the inelastic buckling of pipes in the present study is the nearly rigid saddles used to transmit the load from the

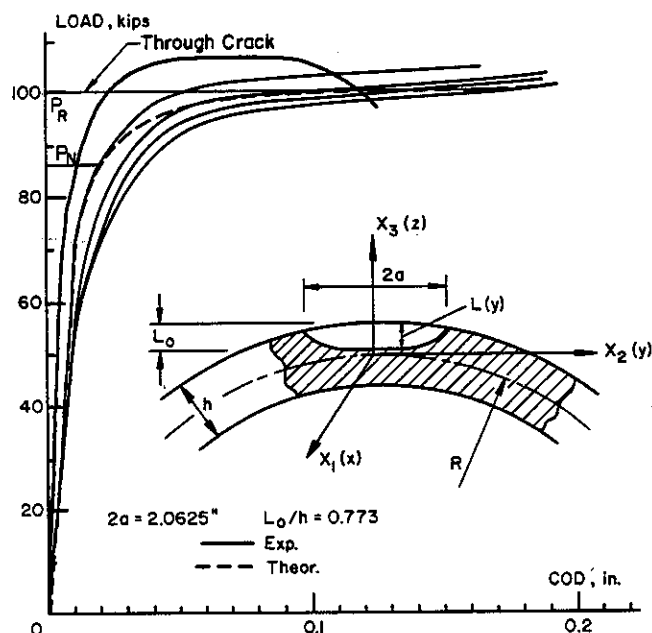


Fig. 25—Transverse load  $P$  vs. COD for pipe # 5

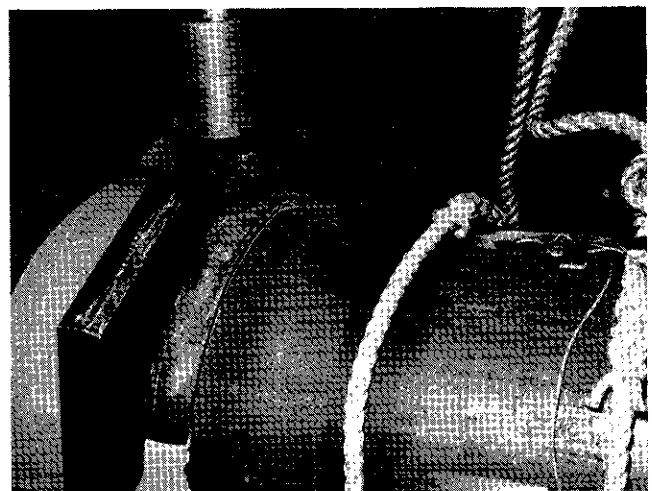


Fig. 27—Buckling of pipe #2 on the compression side

hydraulic jacks to the specimens. There was indeed an indication of slight buckling initiation in all pipes tested. They were all on one side and very near the saddle. The local "bending" in the pipe wall near and at the leading edge of the saddle seems to be one of the main factors for the reduction in the observed instability load. The degree of buckling instability was also responsible for the difference in behavior of the measured load vs. COD curves obtained from pipes #4 and #5 which had nearly identical initial part through fatigue cracks. The buckling in the pipe #5 started at a smaller COD value than in #4 which consequently resulted in the reduction of the load at a comparatively smaller COD value. To give an idea about the comparative behavior of the measured  $P$  vs. COD curves obtained from various pipes they are reproduced in Fig. 28 in superimposed form. Except for the pipe #1 which had a relatively long initial through crack (and to some extent #3 which had an initial through crack), the elastic behaviors (that is the initial parts of the curve) in all pipes seem to be quite similar, whereas buckling played a major role in the inelastic range. Of the six pipes tested only in one (pipe #6) there was no evidence of any structural buckling on the compression side. In this pipe after the net ligament rupture the through crack continued to grow in a slow stable fashion. At some point the clip gage ran out of space and fell and the test was terminated. When the test was stopped the crack (which had an original length of 1.97 in.) was approximately 7 in. long. In the remaining pipes there was very small stable growth of the through crack.

For the pipes tested, Figs. 21–26 also show the load vs. COD relationship obtained from the elastic-plastic analysis described in the Section 3 of this paper. For part-through cracks shown in Figs. 24–26 four calculated curves are given: one for the part-through crack with the profile as given by the fatigue experiment, the second for the corresponding through crack and the third and fourth for intermediate net ligament thicknesses. For a given COD the curve based on the fatigue

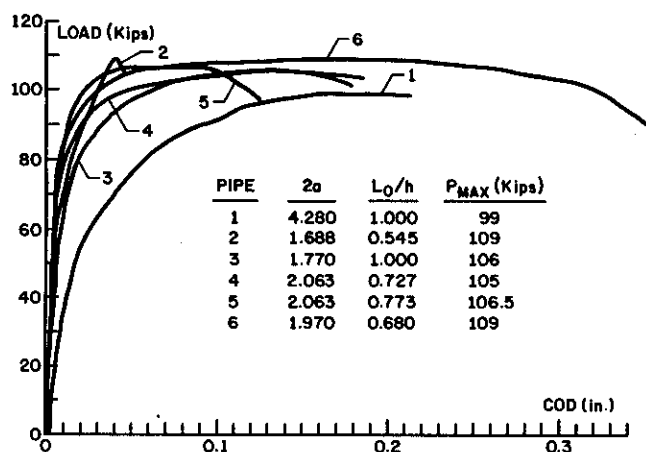


Fig. 28—Transverse load  $P$  vs. COD in the pipes tested as reproduced from the x-y recorder.

crack has the highest and that based on the through crack the lowest values of the load  $P$ . The curves corresponding to the intermediate crack depth fall between these two limiting values. The "net ligament rupture" point (or the load corresponding to the "through crack" initiation)  $P_R$  is marked on the experimental curve (which was obtained from the photocell). Clearly, for loads greater than  $P_R$ , the crack should be treated as a through crack. The initial linear portion of the curves correspond to elastic loading. Between the load  $P_N$  corresponding to the plastic necking or tearing initiation of the net ligament and  $P_R$  corresponding to total net ligament rupture, intermediate values of net ligament thickness must be used to obtain the theoretical  $P$  vs. COD curve.

Again, it should be emphasized that the ductile fracture process involving relatively thin-walled structures and large flaws is very highly geometry-dependent and cannot be characterized by a single parameter. The empirical or semi-empirical models designed for this purpose would generally be satisfactory only for the geometry they were developed. The simple idea underlying the current study is that if one can define or designate a certain parameter which is an adequate measure of the intensity of the applied loads and of the severity of the flaw under conditions of large scale plastic deformations, and the value of which may not be highly sensitive to the details of the elastic-plastic model assumed for the purpose of calculating it, then the asymptotic behavior of this parameter may be used to estimate a gross stability load for the flawed component. As argued before in this paper COD comes perhaps closest to fulfilling the conditions of such a parameter.

The asymptotic behaviors of the experimental and the theoretical  $P$  vs. COD curves are expected to be different. The experimental curve is obtained from a displacement controlled test and hence exhibits a maximum for the load ( $P_{max}$ ). The theoretical COD curves on the other hand possess a true asymptote ( $P = P_{max}$ ). These asymptotic values of  $P$  are the theoretical estimates of the instability load in each pipe. For the six pipes tested, Table 11 shows the comparison of measured and estimated instability loads.

An alternative way of presenting the results may be seen, for example, in Fig. 29 where the normalized COD

Table 11. Experimentally measured and theoretically estimated fracture instability values of Transverse load  $P$  in pipes.

Pipe #	2a	L <sub>0</sub> /h	(P <sub>max</sub> ) <sub>exp</sub> (kips)	(P <sub>max</sub> ) <sub>Theor.</sub>
1	4.280	1.0	99	91
(*) 2	1.688	0.545	109	112
3	1.770	1.0	106	103
4	2.063	0.727	105	102
5	2.063	0.773	106.5	102
6	1.970	0.680	109	105

(\*) Inelastic buckling, no fracture.

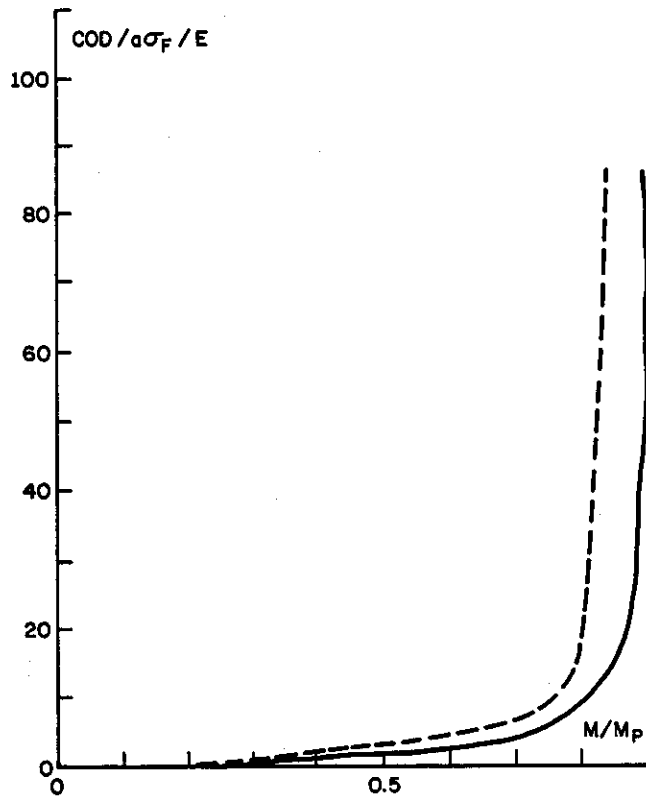


Fig. 29—Normalized COD vs. moment ratio for pipe #6

(with respect to  $a\sigma_F/E$ ,  $a$ ,  $\sigma_F$  and  $E$  being the half crack length, the flow stress, and the Young's modulus) is plotted against the moment ratio  $M/M_P$ . Here  $M$  is the moment applied to the pipe and  $M_P$  is the fully plastic (or collapse) value of  $M$  which is given by

$$M_P = 2\sigma_F \int_0^\pi \int_{R-h/2}^{R+h/2} r^2 \sin \theta dr d\theta$$

$$= \frac{4\sigma_F}{3} \left[ \left( R + \frac{h}{2} \right)^3 - \left( R - \frac{h}{2} \right)^3 \right]. \quad (29)$$

In all pipes tested for ductile fracture, at peak value of the load the region of the shell containing the crack was fully yielded and after the tests were terminated permanent deformations in the form of gross bending was observable. However, the elastic plastic analysis of the crack problem in the pipe was still valid. Considered as a beam, the pipe still had a very large "elastic core" after the extremities were plastically deformed. Thus, unlike the plate problem under similar situations, there was no "net section collapse." Also, in the elastic-plastic shell analysis the end points of the plastic zone in the plane of the crack extended into the elastic region in the pipe.

Originally, it was thought that the net ligament would suddenly become unstable and one may have some dynamic effects on the tearing of the resulting through crack. However, as seen from COD vs.  $P$  records (Fig. 28) in the type of problems under consideration the tearing or necking-tearing process in the net ligament is gradual and, for the circumferential cracks, stable.

Therefore, it does not seem to be practical to talk about a "net ligament instability" load. Since the development of the through crack and its initial growth are stable, the only meaningful instability load is that of the through crack.

#### 4.5 Examination of Fracture Surfaces

As in plates containing a surface crack,<sup>24</sup> in fatigue-cracked pipes subjected to fracture the evidence of considerable necking was observable in the net ligament, particularly from the inside surface of the pipe opposite to the crack. The examination of the two halves of the fractured specimen indicated that after the development of the stretch zone the crack started along the front and slowly propagated in thickness direction. The stability of this phase of the crack propagation was evident from the fact that prior to and during the net ligament rupture (initiation of which was detected by the photo cell) the load was still on the rise. The direction of the crack propagation was perpendicular to the pipe surface. This may easily be seen from the fact that in the net ligament region the two halves of the fractured pipe wall were perfectly symmetric with respect to the original plane of the crack. There is every indication that upon the initiation of ductile tear the crack profile near and at the leading edge maintained its (symmetric) V shape as it propagated through the net ligament. Fig. 19 shows a sketch and Fig. 30 a photograph of the fracture surface.

One of the basic microscopic fracture mechanisms that almost always presents itself in cases of ductile fracture is microvoid coalescence. The stress induced fracture and, in some cases, complex dislocation interactions lead to the formation of microcracks or pores within the stressed component. As the stress level increases these voids grow larger and start coalescing to form a broad crack front. There are, roughly speaking, three main processes for void formation and coalescence which depend on the stress state existing in the component. Under simple uniaxial loading conditions, the microvoids will tend to form in association with fractured particles and/or interfaces and grow out in a plane generally normal to the direction of the applied stress. The resulting "equiaxial dimples" are believed to be related in some fashion to the fracture energy. However, when the failure is predominantly influenced by shear stresses, the voids that nucleate in the manner cited above grow and subsequently coalesce along planes of maximum shear stress. Consequently, these voids tend to be elongated and result in the formation of parabolic depressions on the fracture surface. Finally, if the state of stress is that of combined membrane and bending stresses, again the voids would be elongated, pointing back at the origin of the crack.

From Fig. 30 one may easily distinguish three different zones on the fracture surface, namely the fatigue crack, net ligament rupture, and the through-thickness shear fracture of the pipe wall. Even though both the net ligament and the pipe wall were undergone ductile fracture, their appearance were quite different. The net

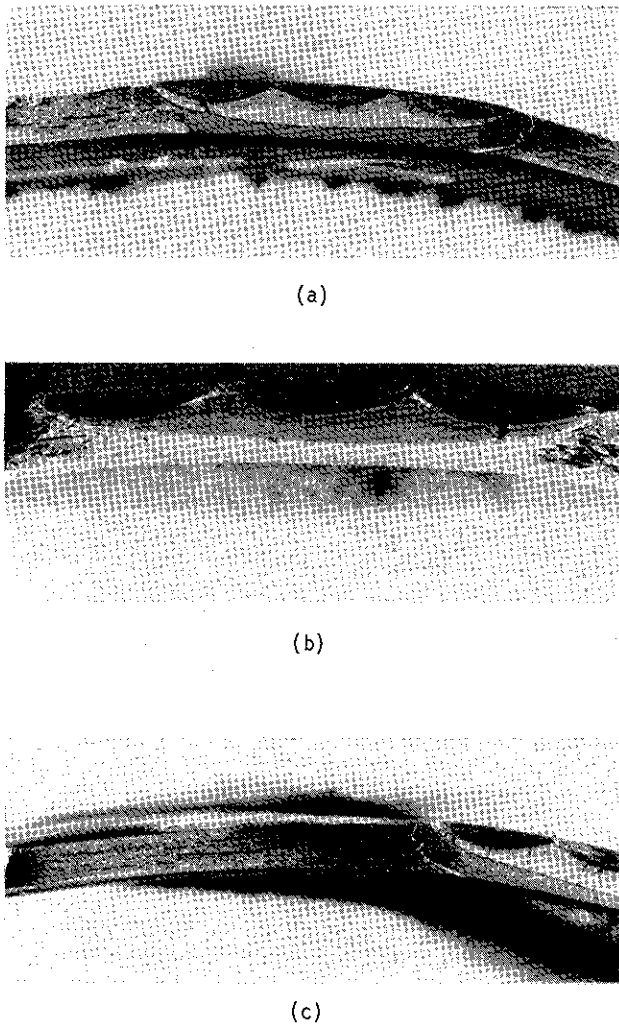


Fig. 30—Various views of the fracture surface of the pipe #6,  $L_0 = 0.68$  h in.,  $2a = 1.97$  in.

ligament appeared to have the structure of a fine-textured dimple fracture and had no signs of delamination. On the other hand, the through-thickness fracture beyond the crack tips had much coarser surfaces and had the appearance of shear fracture of a laminated material with clearly observable delamination cracks (Fig. 30, see, also, Fig. 17b).

For a closer examination of various fracture surfaces photomicrographs were taken at various locations in pipe #6 by scanning electron microscope (SEM). Fig. 19 shows a sketch of the fracture surface of the pipe #6 which indicates the locations of the samples (601, 602, 603, 604) used in SEM. The symbols  $r$ ,  $c$ , and  $c.g.$  shown in Figs. 31–33 refer to the (outward) radial, circumferential, and macroscopic crack growth directions, respectively. The views of the fracture surface opposite to that used in SEM study are shown in Fig. 30. The braze shown in Fig. 19 was part of an effort to use an acoustic emission device for detecting the crack initiation. This attempt did not prove to be very reliable.

The series of photomicrographs shown in Fig. 31 are taken from the sample 603. Fig. 31a shows fatigue surface and part of the stretch zone (marked by A). The

stretch zone and the beginning of the tear region are shown in Fig. 31b. Views further into the tear region are shown in Figs. 31c and d. The orientation of the dimples in these figures indicate that the direction of the crack propagation was radial. On the fracture surface there was no evidence of shear fracture in the net ligament propagating in circumferential direction.

Fig. 32 shows various views of the sample 602. Figs. 32a and b show low magnification photomicrographs of the whole pipe wall and a portion of the peculiar band which was developed during the fracture process. In the section of the pipe wall shown in Fig. 32a the regions of machined surface, fatigue crack, and the ductile fracture surface including the delaminations and the “band” are clearly visible. The band is also seen in Fig. 32b. Figure 32c shows a photomicrograph of the fatigue surface. The stretch zone adjacent to the fatigue surface and the transition region (to ductile fracture) are shown in Fig. 32d. The “band” observed in Figs. 32a and b is also visible (this time in light color) near the crack tips in Fig. 30 and is believed to be due to the interruption of the test momentarily for manual readjustment of the loading jacks.\* This may have caused a crack closure, resulting in “smearing” or “flattening” of the dimples. It is, nevertheless, clear that the bands seen in Fig. 30 along the entire thickness of the pipe correspond to the crack front at a particular time during the propagation of the through thickness fracture.

The photomicrographs of the sample 601 are shown in Fig. 33. Fig. 33a shows the view from a “valley” between delaminations where the voids tend to be more equiaxial. As one climbs along the side of a delamination the shearing effect becomes more visible and the dimples tend to be more elongated (Fig. 33b). The difference between the through-thickness tear in the net ligament and the circumferential tear in the pipe wall seems to be purely a matter of stress state and geometric constraints. Circumferential tear region contains highly pronounced delaminations which may have initiated from the impurities in the steel whereas the net ligament is completely free of such delaminations.

## 5. Conclusions

One of the main conclusions of this study is that in shell structures containing a relatively large initial crack generally the fracture instability load is highly dependent on the overall mechanics of the problem (i.e., the geometry and loading conditions) as well as on the fracture resistance characteristics of the material, and a properly selected and fairly accurately calculated parameter such as COD may be used to estimate the instability load. By examining the results given in Figs. 21–26 and in Table 11 it may be observed that the estimate which may be obtained from the current analysis

\* The drop of the load  $P$  to zero and reloading is not shown in Fig. 26. Fig. 26 was reproduced from the oscilloscope record in which unloading and loading was ignored. However, the corresponding trace in the  $x$ - $y$  recorder shows that the unloading and loading were perfectly elastic, followed the same straight line (in  $P$  vs. COD plane), and there was no sign of any discontinuity or kink in  $P$  vs. COD record.

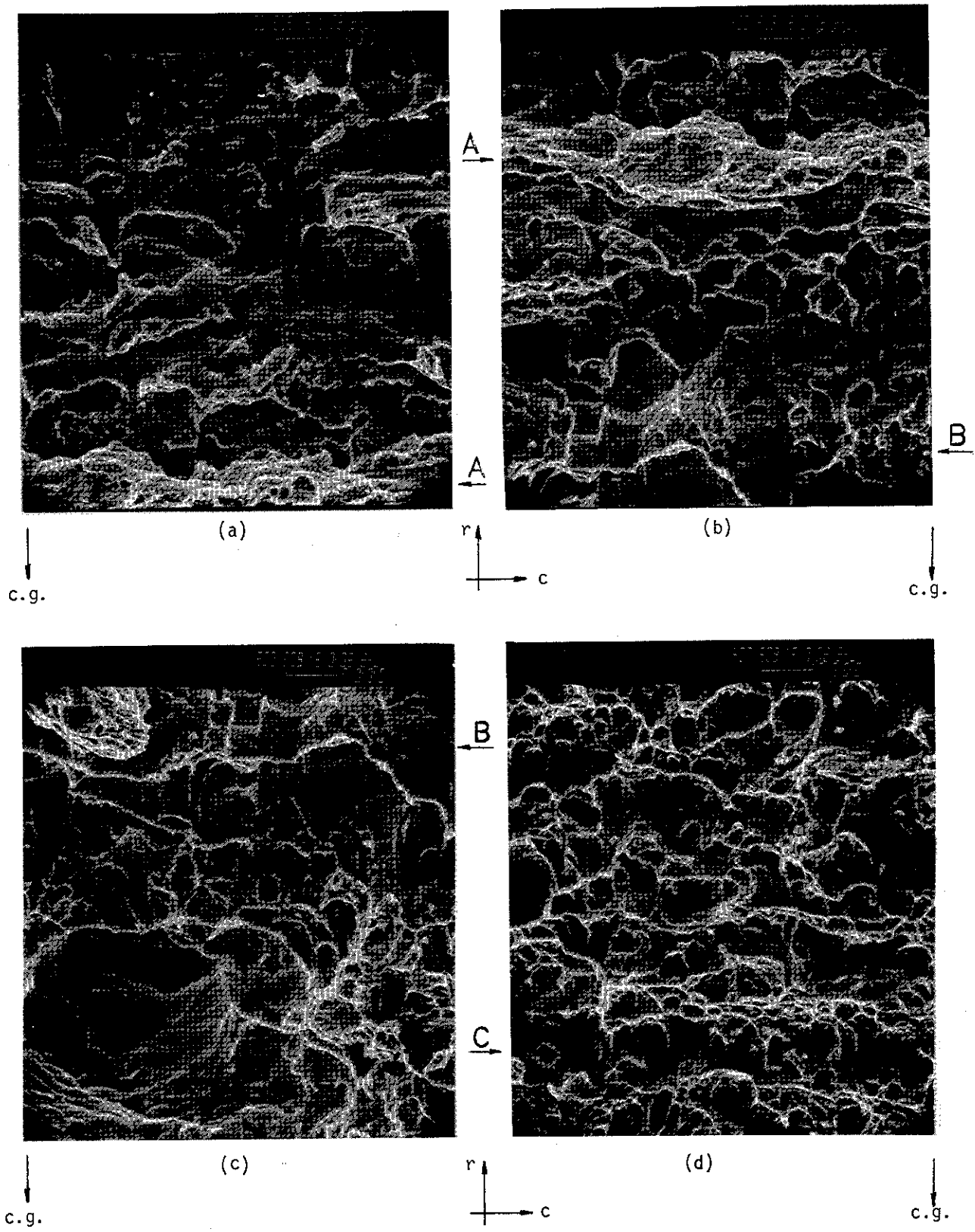


Fig. 31—Scanning electron micrographs (SEM) of the fracture surface at the location 603 (see Fig. 19). (a) fatigue surface and stretch zone (A), (b) stretch zone (A) (overload) and tear region, (c) tear region, (d) further into the tear region (1000X). (*r*: outward radial direction, *c*: circumferential direction, *c.g.*: crack growth direction)

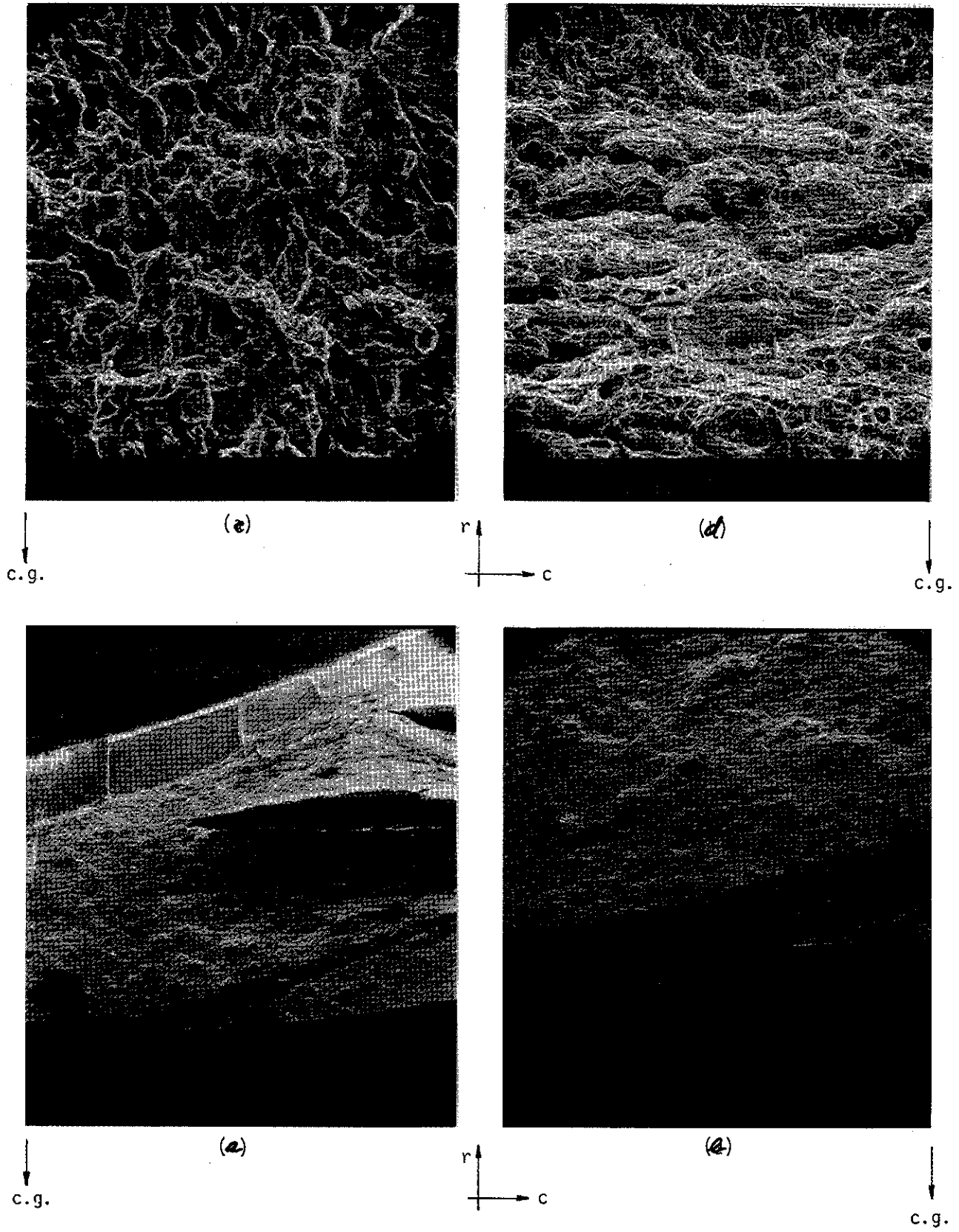


Fig. 32—SEMs of the fracture surface at the location 602 (Fig. 19). (a) Low magnification view from the top: machined surface, fatigue crack, tear region which includes delaminations, the "band," further into the tear region (20X), (b) tear region and the "band" at 50X, (c) fatigue surface at 1000X, (d) stretch zone or transition from fatigue to ductile fracture region at 1000X

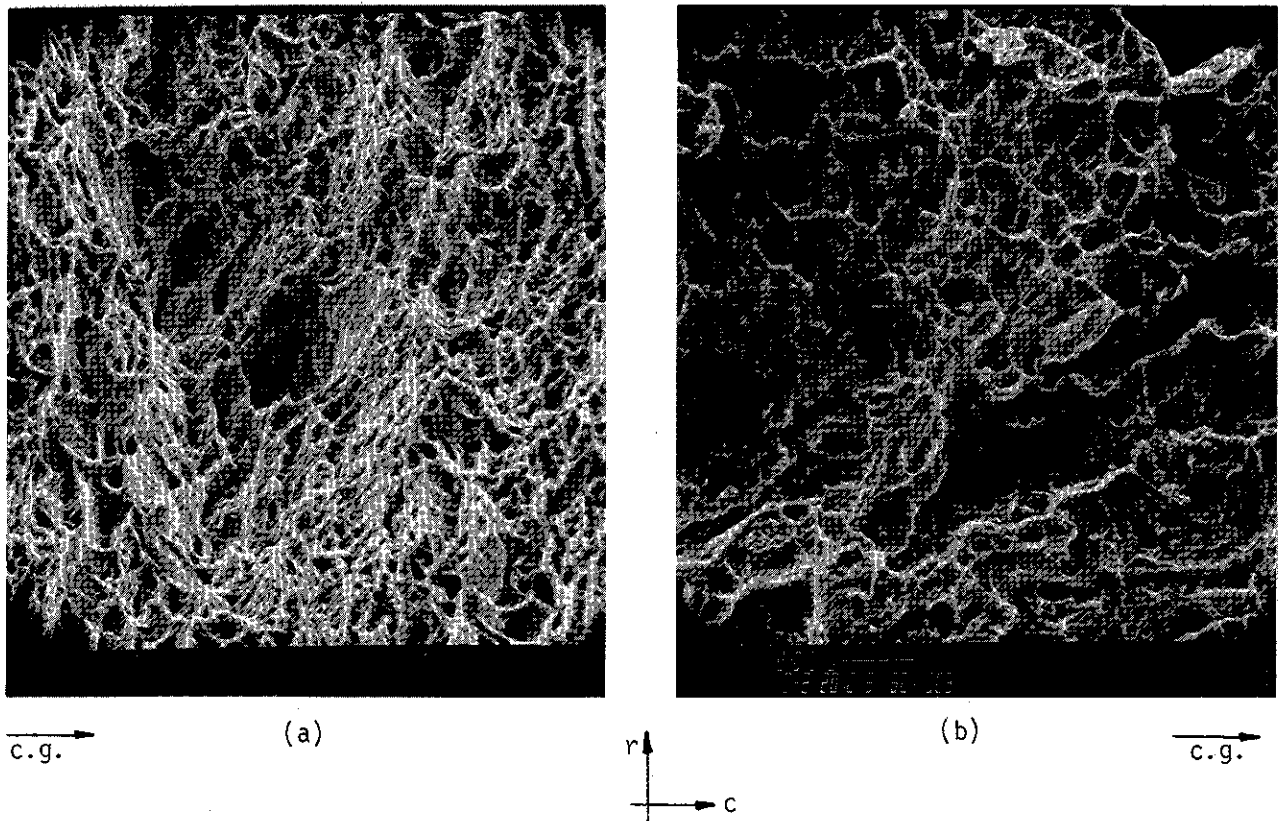


Fig. 33—SEMs of the fracture surface at the location 601 (Fig. 19). (a) In a valley between delaminations, (b) along the side of a delamination (1000X)

appears to be sufficiently close to the instability load and furthermore seems to be consistently conservative. One should also remark that if the tests were performed under “load-controlled” conditions, qualitatively the experimental  $P$  vs. COD curves would have been very similar in behavior to the theoretical curves, in that they would not have had a maximum and would have been asymptotic to  $P = P_{max}$  lines.

As indicated before there was considerable necking in the net ligament from inside the pipe wall, the crack growth through the net ligament was perpendicular to the pipe surface and was stable, and after the initiation of ductile tear the crack profile near and at the leading edge maintained its (symmetric) V shape as it propagated. On the other hand, after the net ligament rupture the through crack propagated essentially in shear mode between planes formed by delamination cracks. Even though Fig. 30 appears to indicate a finer textured fracture surface for the net ligament, scanning electron micrographs showed that both the net ligament and the wall were undergone basically the same dimple fracture.

The particular X60 line pipes which were subjected to four point bending and which contained a part-through circumferential fatigue crack on the tension side provided to be very highly resistant to ductile fracture. Even though it was possible to rupture the net ligament (i.e., the pipe wall under the crack) in all but one of the pipe specimens, the gross failure under

gradually increased static bending occurred mostly as a result of inelastic buckling of the pipe wall on the compression side rather than fracture instability (i.e., unstable crack growth) on the tension side. The one pipe specimen in which the net ligament did not rupture and in which there was severe buckling on the compression side contained a relatively shallow fatigue crack. In one specimen there was no sign of buckling and the structural failure resulted from fracture instability. In all cases the theoretical model gave conservative estimates for the fracture instability load.

The research program, which was partially supported by NSF and NASA-Langley, led to the publication of the following articles:

“Transverse Shear Effect in Circumferentially Cracked Cylindrical Shells,” *Quarterly of Applied Mathematics*, Vol. 37, 1979, pp. 239–258 (F. Delale and F. Erdogan).

“Line-Spring Model for Surface Cracks in a Reissner Plate,” *Int. J. Engng. Science*, Vol. 19, pp. 1331–40, 1981 (F. Delale and F. Erdogan).

“Ductile Fracture of Pipes and Cylindrical Containers with a Circumferential Flaw,” *J. Pressure Vessel Technology, Trans. ASME*, Vol. 103, pp. 160–168, 1981 (F. Erdogan and F. Delale).

“Elastic-Plastic Problem for a Plate with a Part-Through Crack under Extension and Bending,” *Int. J. Engng. Science*, Vol. 20, 1982 (M. B. Civelek and F. Erdogan).

"Application of the Line-Spring Model to a Cylindrical Shell Containing a Circumferential or an Axial Part-Through Crack," *J. Applied Mechanics, Trans. ASME*, Vol. 49, 1982, pp. 97-102 (F. Delale and F. Erdogan).

"Stress Intensity Factors in a Hollow Cylinder Containing a Radial Crack," *Int. J. Fracture Mechanics*, Vol. 19, 1983 (F. Delale and F. Erdogan).

"The Elasticity Problem for a Thick-Walled Cylinder Containing a Circumferential Crack," *Int. J. Fracture Mechanics*, Vol. 19, 1983 (H. F. Nied and F. Erdogan).

"The Transient Thermal Stress Problem for a Circumferentially Cracked Hollow Cylinder," *Journal of Thermal Stresses*, 1983 (H. F. Nied and F. Erdogan).

"Elastic-Plastic Fracture of Cylindrical Shells Containing a Part-Through Circumferential Crack," ASME paper to be presented at 1982 Winter Annual Meeting (F. Erdogan and H. A. Ezzat).

## 6. References

1. Reich, M. and Esztergar, E. P., "Compilation of References, Data Sources, and Analysis Methods for LMFBR Piping System Components," Brookhaven National Laboratory, BNL-NUREG-50650, March 1977.
2. *The Surface Crack*, Swedlow, J. L., ed., ASME, New York, 1972.
3. Raju, I. S. and Newman, J. C., Jr., "Improved Stress Intensity Factors for Semi-Elliptic Surface Cracks in Finite Thickness Plates," NASA TMX-72825, 1977.
4. Erdogan, F., "Crack Problems in Cylindrical and Spherical Shells," in *Plates and Shells and Cracks*, Sih, G. C., ed., Noordhoff Int. Publ., Leyden, 1977.
5. Erdogan, F. and Ratwani, M., "Plasticity and Crack Opening Displacement in Shells," *Int. J. Fracture Mechanics*, Vol. 8, 1972, pp. 413-426.
6. Kobayashi, A. S., Polvanich, N., Emery, A. F. and Love, W. J., "Inner and Outer Cracks in Internally Pressurized Cylinders," *J. Pressure Vessel Technology, Trans. ASME*, Vol. 99, 1977, pp. 83-89.
7. Rolfe, S. T. and Barsom, J. M., *Fracture and Fatigue Control in Structures*, Prentice-Hall, 1977.
8. *Fracture Toughness Evaluation by R-Curve Methods*, ASTM-STP 527, 1973.
9. Newman, J. D., Jr., "Fracture Analysis of Surface and Through-Cracked Sheets and Plates," *J. Engng. Fracture Mechanics*, Vol. 5, 1973, pp. 667-689.
10. Erdogan, F., "Ductile Fracture Theories for Pressurized Pipes and Containers," *Int. J. Pressure Vessels and Piping*, Vol. 4, 1976, pp. 253-283.
11. Kiefner, J. P., Maxey, W. A., Eiber, R. J. and Duffy, A. R., "Failure Stress Levels of Flaws in Pressurized Cylinders," in ASTM-STP 536, 1973, pp. 461-481.
12. Wilkowski, G. M. and Eiber, R. J., "Review of Fracture Mechanics Approaches to Defining Critical Size Girth Weld Discontinuities," *WRC Bull.* 239, July 1978.
13. Reed, R. P., McHenry, H. I. and Kasen, M. B., "A Fracture Mechanics Evaluation of Flaws in Pipeline Girth Welds," *WRC Bull.* 245, Jan. 1979.
14. *Crack Propagation in Pipelines*, Inst. Gas Eng., London, 1974.
15. Popelar, C., Rosenfield, A. R. and Kanninen, M. F., "Steady-State Crack Propagation in Pressurized Pipelines," *J. Pressure Vessel Technology, Trans. ASME*, Vol. 99, 1977, pp. 112-121.

16. Erdogan, F., Delale, F. and Owczarek, J. A., "Crack Propagation and Arrest in Pressurized Containers," *J. Pressure Vessel Technology, Trans. ASME*, Vol. 99, 1977, pp. 90-99.

17. Krenk, S., "Influence of Transverse Shear on an Axial Crack in a Cylindrical Shell," *Int. J. Fracture*, Vol. 14, 1978, pp. 123-143.

18. Newman, J. C. and Raju, I. S., "Stress Intensity Factors for Internal Surface Cracks in Cylindrical Pressure Vessels," NASA Technical Memorandum 80073, July 1979.

19. McGowan, J. J. and Raymund, M., "Stress Intensity Factor Solutions for Internal Longitudinal Semi-Elliptical Surface Flaws in a Cylinder under Arbitrary Loadings," *Fracture Mechanics*, ASTM, STP 677, 1979.

20. Heliot, J., Labbens, R. C. and Pellissier-Tanon, A., "Semi-Elliptic Cracks in a Cylinder Subjected to Stress Gradients," *Fracture Mechanics*, ASTM, STP 677, 1979, pp. 341-364.

21. Delale, F. and Erdogan, F., "Application of the Line Spring Model to a Cylindrical Shell Containing a Circumferential or Axial Part-Through Crack," *J. Appl. Mech., Trans. ASME*, Vol. 49, 1982, pp. 97-102.

22. Delale, F. and Erdogan, F., "Transverse Shear Effect in a Circumferentially Cracked Cylindrical Shell," *Quart. Appl. Mathematics*, Vol. 37, 1979, pp. 239-258.

23. Erdogan, F. and Ratwani, M., "Fatigue and Fracture of Cylindrical Shells Containing a Circumferential Crack," *Int. J. of Fracture Mechanics*, Vol. 6, 1970, pp. 379-389.

24. Erdogan, F., "Theoretical and Experimental Study of Fracture in Pipelines Containing Circumferential Flaws," Final Report, U.S. Department of Transportation Contract DOT-RC-82007, Aug. 1982.

25. Yahsi, O. S., "Effect of Transverse Shear and Material Orthotropy in a Cylindrical Shell Containing an Arbitrarily Oriented Crack," Ph.D. Dissertation, Lehigh University, 1981.

26. Timoshenko, S. P. and Gere, J. M., *Theory of Elastic Stability*, 2nd Ed., McGraw-Hill, New York, 1961.

27. Vinson, J., *Structural Mechanics: Behavior of Plates and Shells*, J. Wiley, 1974.

28. Vosikovskiy, O., "Effects of Stress Ratio on Fatigue Crack Growth Rates in X70 Pipeline Steels in Air and Salt Water," *Journal of Testing and Evaluation*, Vol. 8, 1980, pp. 68-73.

29. Wilkowski, G. M. and Eiber, R. J., "Evaluation of Tensile Failure of Girth Weld Repair Grooves in Pipe Subjected to Offshore Laying Stresses," *Journal of Energy Resources Technology, Trans. ASME*, Vol. 103, 1981, pp. 48-55.

## 7. Acknowledgments

The authors greatly appreciate the contributions made to this study by the following: F. Delale, H. F. Nied, M. B. Civelek, A. C. Kaya, S. Baskan, and R. Roberts.

Special thanks are also extended to Professor R. Slutter for providing the facilities of Lehigh University's Fritz Engineering Laboratory for the experimental part of this study and for his valuable advice in setting up and in carrying out the tests, Professor A. W. Pense and Dr. B. R. Somers for their help in the fractographic studies, Dr. Orringer of the Transportation Systems Center for his advice and encouragement during the period of this research program, Dr. M. Lauriente of D.O.T. for his interest and encouragement, Dr. J. H. Gross of U.S. Steel for providing the X-70 line pipe material for plate experiments, and Stupp Brothers, Inc. of Saint Louis, Missouri for providing the X-60 line pipes for the pipe experiments.

